JOURNAL OF GEOPHYSICAL RESEARCH, VOL. 100, NO. A7, PAGES 11,981–11,999, JULY 1, 1995

# Kinetic structure of rotational discontinuities: Implications for the magnetopause

D. Krauss-Varban, H. Karimabadi, and N. Omidi[1]

Department of Electrical and Computer Engineering, University of California at San Diego, La Jolla

**Abstract.** Magnetic field rotations in the high ion beta magnetosheath that are part of the magnetopause structure are expected to have only a small normal component. We have studied the properties of rotational discontinuities (RDs) under these conditions, viewed as the limit of weak intermediate shocks (ISs), by performing hybrid simulations with a reflecting wall boundary condition (piston method). With this dynamic formation, the sense and size of rotation are not arbitrarily predetermined, but rather evolve from the given upstream (magnetosheath) and downstream (magnetospheric) boundary conditions, similar to what takes place at the magnetopause. This work focuses on several aspects: the observed minimum shear of RDs, their width, their internal signature, and their relation to ISs in isotropic plasmas. Our simulation results are in agreement with the minimum shear observations, that is, the RDs choose the sense of rotation that corresponds to the minimum angle between the upstream and downstream field vector. The RDs are stable, with a unique scale size. Typical gradient scale half widths are one to four ion inertial lengths with a total width up to ten times of that, in agreement with magnetopause observations. We develop a generalized fluid theory of RDs and discuss the characteristic internal signatures of the rotational layer, comparing the kinetic simulation results to predictions from the generalized fluid theory. The results show that ion inertia, anisotropic pressure, finite Larmor radius effects, nonzero ion heat flux, and reflected ions all contribute to the signatures of RDs on kinetic scales. The RDs may have upstream or downstream wave trains, which become weak for high ion beta and small normal components of the magnetic field. We explain the presence and direction of wave trains in terms of the kinetic properties of the Alfvén/ion-cyclotron mode. Away from the RD limit there is a smooth transition to weak intermediate shocks, which have small jumps close to expected Rankine-Hugoniot values. Apart from that, there are few kinetic plasma signatures that distinguish RDs from their neighboring ISs. However, noncoplanar ISs evolve in time into thin RDs. Using the properties of RDs and ISs, we make specific suggestions how these discontinuities can be distinguished observationally in the case of an isotropic plasma.

## 1. Introduction

Many observations of the magnetopause current layer have shown that it can have a finite normal magnetic field component and at times locally resembles a rotational discontinuity (RD) [*Sonnerup et al.*, 1981; *Berchem and Russell*, 1982a, b; *Gosling et al.*, 1990, 1991]. Rotational structures like RDs are expected to form when the magnetopause is open and daytime reconnection of magnetosheath field lines with formerly closed dipole field lines takes place [e.g., *Vasyliunas*, 1975]. In this paper the kinetic properties of RDs are investigated for plasma conditions that are typical for the magnetopause. These are a relatively high ion beta ($\beta_i$, ratio between the ion thermal pressure and the magnetic pressure) and a small normal component of the ambient magnetic field. In addition to questions regarding the existence, stability, and signatures of RDs under these conditions, we are interested in the relation of RDs to intermediate shocks (ISs). The kinetic structure of ISs is investigated in great detail in a companion paper [*Karimabadi et al.*, this issue], hereafter referred to as paper 1.

The properties of RDs in MHD theory for an isotropic plasma can be summarized as follows. RDs are discon-

[1] Also at California Space Institute, University of California at San Diego, La Jolla.



Paper number 94JA03034.
0148-0227/95/94JA-03034$05.00

tinuities that rotate the transverse magnetic field and the transverse, field-aligned flow velocity; they propagate with a velocity $v_{An} = v_A \cos\theta_{Bn}$, where $v_A = v_{Ao} = B_o(4\pi\rho_o)^{-1/2}$ is the (upstream) Alfvén velocity, $B_o = |\mathbf{B}_o|$ is the upstream magnetic field magnitude, $\rho_o$ is the upstream mass density, and $\theta_{Bn}$ is the acute angle between $\mathbf{B}_o$ and the normal $\mathbf{n}$ of the discontinuity. There is no jump of the plasma quantities across RDs in an isotropic plasma, thus the index o indicating upstream quantities can be omitted. In MHD theory RDs can have arbitrary rotation angles. For example, if the downstream transverse magnetic field makes an angle $\alpha_*$ with the upstream transverse magnetic field, rotational solutions are allowed of the form $\alpha = \alpha_* + 2\pi n$ for all (positive and negative) integers $n$. A positive $\alpha$ corresponds to left-handed (ion sense) rotation, and a negative $\alpha$ refers to right-handed (electron sense) rotation. Observations have shown that both senses of rotation actually exist, but in particular such that the magnetic field rotates in the direction of minimum shear, $|\alpha| \leq 180°$ [*Berchem and Russell,* 1982b]. This finding is also supported by observations of RDs in the solar wind [*Neugebauer and Buti,* 1990]. MHD theory cannot explain the observed minimum shear, since in MHD RDs have no internal structure. Similarly, MHD theory cannot determine the thickness of RDs.

There has been some hope that generalized fluid theories may give a better physical description of RDs. It has been suggested that in more general fluid theories only a specific sense of rotation is allowed. For example, *Hau and Sonnerup* [1991] did not find any solutions for ion sense rotations, when ion inertia and finite Larmor radius (FLR) effects were included in the calculations. Also, their calculations indicated that RDs exist only for specific combinations of upstream parameters and rotation angles. However, such findings are not supported by observations and do not agree with simulations [*Krauss-Varban,* 1993]. Here we develop a generalized fluid theory of RDs and show that different results are obtained when ion inertia and FLR corrections (which need to be small for the equations to be valid) are consistently carried through to first order. Then, as in ideal MHD, both senses of rotation are proper solutions, and there is no particular width. We compare the internal signatures that are predicted by this fluid theory under various assumptions for the fluid with our kinetic simulations. We find that application of a generalized fluid theory is problematic because it does not describe effects due to reflected and trapped ions, and new FLR corrections would need to be calculated for the specific conditions that are prevalent in the collisionless plasma.

Some of the earliest hybrid simulations (kinetic ions, fluid electrons) of RDs suggested that rotations with $|\alpha| > 180°$ are unstable and disintegrate into their minimum shear counterparts [*Swift and Lee,* 1983]. A more detailed simulation study by *Krauss-Varban* [1993] showed that ion and electron sense rotations with $|\alpha| > 180°$ evolve in different ways. While the rate of evolution depends on the RD's thickness, ion sense rotations can be metastable (i.e., no significant change for many $100\ \Omega^{-1}$, where $\Omega$ is the ion cyclotron frequency). Such configurations are sensitive to external perturbations [*Krauss-Varban,* 1994]. Although these simulations have demonstrated mechanisms by which minimum shear solutions can be approached, they have not explained the universality of the minimum shear observations.

In hybrid simulations RDs can be initialized with arbitrary thickness. However, *Goodrich and Cargill* [1991] reported what appeared to be a threshold thickness of the order of a few ion inertial lengths. If initialized below that, the RDs would simply widen to this scale. *Krauss-Varban* [1993] showed that for finite $\beta_i$, this minimum thickness is at least for a limited parameter regime determined by the combined ion inertial length and ion gyroradius scales. Observations at the magnetopause have shown that the width of the rotational layer is consistently of the order of several ion gyroradii [*Sonnerup and Ledley,* 1979; *Berchem and Russell,* 1982a]. Thus, only the minimum obtainable thickness of the above "nondynamic" hybrid simulations is consistent with magnetopause observations, a fact that has not been explained. Note that deep in the magnetosheath, the proton inertial length $c/\omega_p$ may vary between 40 and 80 km. Since the ion beta is typically $1/4 \lesssim \beta_i \lesssim 4$, the ion gyroradius $\rho_{Li} = (\beta_i)^{1/2}\, c/\omega_p$ would usually be at most a factor of two smaller or larger than $c/\omega_p$.

Basically, the previous simulation studies have suffered from an arbitrariness in the sense that they allow RDs of any total rotation (apart from further evolution for sufficiently thin initializations) and any thickness (beyond a certain minimum thickness), both of which are not supported by observations. These types of simulations were performed by prescribing a particular field rotation and gradient scale at the beginning of the computation, which we term nondynamic. Exceptions are simulations by *Omidi* [1991], in which unique RDs formed as part of a solution of multiple discontinuities to a more general Riemann problem, and more recent studies geared toward ISs by *Karimabadi and Omidi* [1992] and *Lin and Lee* [1993].

Here we argue that RDs at the magnetopause may be best viewed as part of the solution to a general Riemann problem. For such conditions, the piston method is most appropriate. This setup is dynamic in the sense that no gradient scale, internal structure, or sense of rotation is prescribed, but rather the discontinuities evolve self-consistently from the boundary conditions. We address the questions listed above with one-dimensional hybrid simulations. One may expect that the piston method simulations should result in discontinuities with a well-defined width, and that is indeed the case. The thickness agrees with the magnetopause observations. Moreover, these thin RDs have always minimum shear rotations (sometimes after a short evolution time). In short, such simulations remove the arbitrariness inherent to the nondynamic method.

In the piston method it is straightforward to study RDs directly as the limit of weak intermediate shocks (ISs) and to study the signatures that distinguish ISs

from RDs. ISs had been thought to be nonexistent for a variety of reasons (see the detailed discussion by *Wu* [1990]). However, using MHD simulations, *Wu* [1988] showed that ISs do indeed exist in dissipative MHD. There has been some controversy because in resistive MHD steady state RDs cannot exist. This is because the entropy does not change across RDs, while at the same time there is dissipation associated with any finite width structure in resistive MHD. However, such arguments are different in a collisionless plasma, in which any resistivity or viscosity has to be provided for self-consistently by wave-particle interaction. It is therefore clear that a kinetic approach is required to answer questions of structure and stability in a collisionless plasma.

Dissipative MHD also allows for noncoplanar ISs ($|\alpha| \neq 180°$). However, these so-called time-dependent intermediate shocks (TDISs) must necessarily evolve in time because the conservation equations do not allow steady state noncoplanar solutions except for RDs. Nevertheless, the timescales for this process may be large, and in principle the findings by *Wu* [1988, 1990] have opened the question whether the magnetopause field rotation is really associated with an RD or an IS. Consequently, part of the purpose of this work is to address the respective signatures of RDs and (subfast) ISs, and to discuss their stability and existence in a collisionless plasma. A full description of weak and strong ISs for magnetopause conditions is given in paper 1. Here ISs are discussed only as far as relavant to our comparison to RDs. We show that with careful simulations it is possible to distinguish between RDs and weak ISs although the jumps associated even with the highest Mach number ISs can be quite small.

The outline of this paper is as follows. Details of the method and numerics are given in section 2, which also provides an overview of the expected Rankine-Hugoniot solutions. Because of the number of issues addressed, we have separated the main part of the paper into two sections, the first one (section 3) presenting the results of the simulations, the second one (section 4) giving detailed explanations of the physics entailed, also in view of magnetopause observations. The topics described in section 3 are minimum shear, hodograms and wave trains, dependence on the rotation angle, stability, and the relation to TDIS. In section 4 the RD signatures are compared to predictions from generalized fluid theory in order to get a better insight into the kinetic processes involved. The physics of the internal structure, scale sizes and wavetrains are discussed in great detail. The analytical theory of generalized fluid solutions of RDs is described separately in the Appendix. The results of our study are summarized in section 5.

## 2. Simulation Setup and Rankine-Hugoniot Expectations

The use of hybrid simulations, which treat the ions kinetically but describe the electrons as a massless fluid, is justified because we are interested in structures on ion spatial and temporal scales. A recent description of the hybrid code has been given by *Winske and Omidi* [1993]. The coordinate system we use is the same as that used by *Krauss-Varban* [1993] and in paper 1. The simulation axis is along $x$ and the upstream magnetic field is in the $x$-$z$ plane. The rotation angle $\alpha$ is measured from the $z$ axis through positive $y$. With the normal magnetic field component pointing in the $+x$ direction, this gives left-handed (LH, ion sense) rotations for positive $\alpha$ and right-handed (RH, electron sense) rotations for $\alpha < 0$.

In the piston method, plasma is injected at the left-hand side of the simulation box, while reflecting boundary conditions are employed at the right-hand side. The right-hand magnetic field values and the injection speed are determined by the Rankine-Hugoniot relations. A discontinuity will form at the right and propagate upstream to the left, such that the simulation frame is at rest relative to the downstream plasma, as far as the normal velocity is concerned. RDs are the limiting case of weak ISs, that is, the upstream and downstream speed are the same and no injection is required. Still, the field rotation that is initially only present as a boundary condition will propagate upstream and form an RD with velocity $v_{An} \simeq v_A \cos\theta_{Bn}$.

Figure 1 shows the Rankine-Hugoniot diagram [cf., *Hau and Sonnerup*, 1989] for a total $\beta$ of 1.2 and a normal angle with respect to the magnetic field of $\theta_{Bn} = 80°$. Here both ions and electrons are assumed to be adiabatic with specific heat ratio 5/3. In this type of diagram the upstream squared Alfvén Mach number $(v_{x0}/v_{A0}\cos\theta_{Bn})^2$ is plotted against the downstream squared Alfvén Mach number, with $v_x$ being the normal flow velocity. Note that the Alfvén Mach number is variously defined with or without the factor $\cos\theta_{Bn}$ in the denominator. Here we write all quantities in

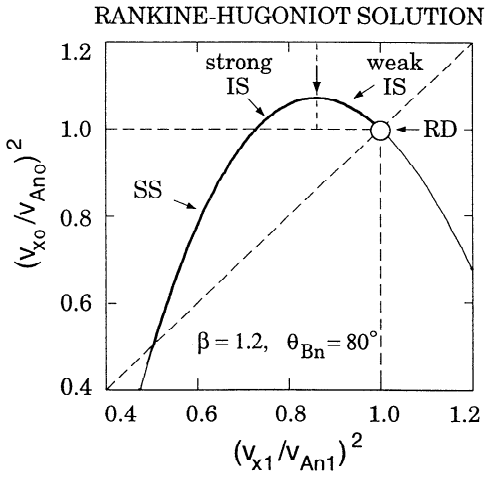


**Figure 1.** Solution curve to the Rankine-Hugoniot equations for a total plasma beta $\beta$ and shock normal angle $\theta_{Bn}$ as indicated. Shown is the upstream squared Alfvén Mach number (subscript o) as a function of the downstream value (subscript 1), where $v_{An} = v_A \cos\theta_{Bn}$. The labels indicate the regions of the slow shock (SS) and strong and weak intermediate shocks (IS) as well as the rotational discontinuity (RD) limit. The region below the diagonal is unphysical.

terms of the normal component of the Alfvén velocity $v_{An} = v_A \cos\theta_{Bn}$ to avoid confusion. A subscript o refers to the upstream, 1 to the downstream, and for RDs we usually omit the subscript. Only a portion of the Rankine-Hugoniot diagram is shown in Figure 1; fast mode shock solutions would be situated at higher Mach numbers where the curve turns upward again. Solutions below the diagonal are unphysical. RDs are situated at the intersection of unit values, that is, the upstream and downstream normal flow speed are both $v_A \cos\theta_{Bn}$. Slow shocks (SSs) are located on the part with sub-Alfvénic upstream velocity. For a given upstream flow speed, two IS solutions, the strong IS and the weak IS are possible. A faster downstream speed and thus less thermalization is associated with the weak IS, which has the RD as its limit. Note that the maximum Mach number IS has an upstream velocity that differs only by a few percent from the RD velocity.

Figure 2 shows the maximum IS Mach number as a function of the plasma beta and $\theta_{Bn}$. Clearly, for typical magnetopause conditions ISs only exist over a small range of Mach numbers close to unity. Figure 3 shows jumps of the magnetic field ($B$), ion temperature ($T_i$), and density ($n$) for the same plasma conditions as in Figure 1 and as a function of the upstream speed, expressed as the percentage difference to the RD velocity (the maximum Mach number IS corresponds to about 3.5%). From Figure 3a it can be seen that expected jumps in these quantities are at most $\sim$ 10 to 30%. The behavior close to the RD limit is difficult to see, so in Figure 3b the percentages $\Delta T_i$ and $\Delta B$ are normalized with the jump in the density $\Delta n$, also in percent. While these jumps are nearly a factor of two larger than those in the density, it is important to note that they are still of the same order of magnitude as the density jump. Thus, for an IS in an isotropic plasma, we expect to see jumps in all three quantities. Although expected jumps are small, they can be important concerning the interpretation of heating at the magnetopause [e.g., *Gosling et al.*, 1991].

Considering the above constraints, the simulations have to be carried out and evaluated very carefully to distinguish RDs from weak ISs. Of course, at a certain level the distinction between the two is esoteric. For example, we may call a discontinuity for all practical purposes an RD if the jumps are below 1 to 2%. To achieve this accuracy, we use 200 to 400 particles per cell in the simulations, and at times make use of a "time-averaged epoch analysis," in which we average quantities in the rest frame of the discontinuity over a time period, to improve the statistical significance and suppress random fluctuations. The simulation box size chosen is sufficiently large such that initial perturbations (which can reflect from the upstream boundary) do not reach the discontinuity. We typically run the simulations 600 to 1000 $\Omega^{-1}$ (inverse ion cyclotron frequencies).

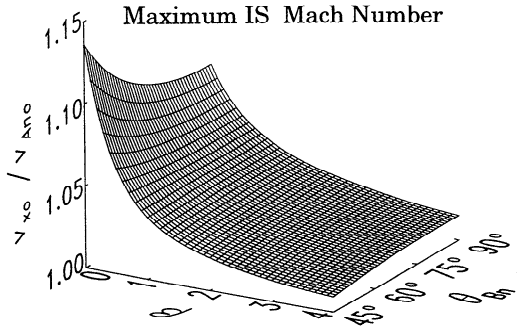


**Figure 2.** Maximum value of the IS Alfvén Mach number (compare Figure 1) as a function of $\beta$ and $\theta_{Bn}$. Note the small values in the high $\beta$ / large $\theta_{Bn}$ regime typical for the magnetopause.

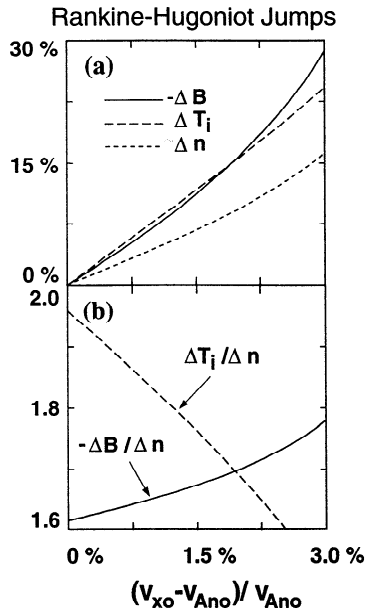


**Figure 3.** Typical weak IS jumps from fluid theory as a function of the IS speed (expressed as percentage deviation from the ideal RD speed $v_{Ano}$) for plasma parameters as indicated. (a) Jumps of the magnetic field $B$, the ion temperature $T_i$, and the density $n$. (b) Relative jumps of $B$ and $T_i$ compared to those of the $n$. Note that even in the RD limit (left side of the Figure) all predicted jumps are roughly comparable.

When referring to the scale size of the solutions, one has to keep in mind the distinction between a total width and the width of the current layer. We measure the current layer thickness $\ell$ as the half width of the gradient in the field component that experiences most of the change (usually $B_z$ here). The total width can be defined as a measure of the region over which the plasma deviates significantly from the upstream and asymptotic downstream, here always excluding any wave train. Although mathematically less rigorous, it can usually be stated within a margin of $\pm 15\%$.

While we have performed simulations for a variety of plasma betas and angles $\theta_{Bn}$ most results presented in the next section are for the two angles $\theta_{Bn} = 60°$ and 80°, with ion betas $\beta_i = 1.0$ to 4.0, and an electron beta of $\beta_e = 0.2$, respectively. We have executed simulations with rotation angles $\alpha = \pm 90°$, $\pm 120°$, $\pm 160°$,

$\pm 170°$, and $\pm 180°$. The reader is referred to *Vasquez and Cargill* [1993] for a discussion of RDs with small $\theta_{Bn}$ and $\beta_i$. Although an ion temperature anisotropy is commonly observed in the magnetosheath upstream of the magnetopause, it is not considered in the present paper. This simplifies the evaluation of jumps at the discontinuity and enables the detection of only slight occurrences of heating. The effect of upstream anisotropy has been discussed by *Omidi* [1991] and will be further analyzed in forthcoming work.

## 3. Simulation Results

We address two groups of questions: those related to the characteristics of RDs and those relevant to stability, dissipation, and the relation of RDs to ISs. In the following sections we present simulation results for noncoplanar and coplanar rotations for both the electron and ion sense. We demonstrate that RDs are stable and show an important difference between the internal signatures depending on the sense of rotation. We also address the width of the transition and its scaling with plasma parameters, whether there is a finite jump in the plasma quantities, and the relation of the RD solutions to weak ISs. Comparison of the internal perturbations with predictions from fluid theory is deferred to the discussion in section 4. There we also explain the phenomenology of hodograms and wave trains in terms of the properties of the Alfvén/ion-cyclotron mode.

### 3.1. Noncoplanar Rotations

In the noncoplanar regime, dissipative MHD predicts that ISs should exist but be time-dependent, approaching infinitely thick RDs in the time asymptotic limit. In paper 1 we have shown that both weak and strong noncoplanar ISs do indeed form; weak TDIS only form as long as the rotation angle is not too far from 180°. However, contrary to the MHD results, these structures retain a finite, more or less fixed thickness of the current layer while slowly evolving into RDs. Here we find that the RD limit coexists with the IS solutions, and that the scale sizes of the weak ISs are similar to their RD limit.

**Minimum shear.** First we show that both senses of rotation exist including the coplanar limit, and that our dynamic formation always leads to the minimum shear solution. When the boundary conditions are chosen such that $\alpha < 0$, a typical electron sense hodogram (see work by *Goodrich and Cargill* [1991] and examples below) forms within several $\Omega^{-1}$. For $\alpha > 0$ typical ion sense hodograms form quickly when the angle is not close to 180°. Close to the coplanar case, at first an RD $|\alpha| > 180$ with a hodogram more typical of an electron sense RD may form, which then reverts to the minimum shear solution. An example of this is shown in Figure 4, for $\alpha = 170°$, $\theta_{Bn} = 60°$, and $\beta_i = 1.0$. The Figure displays the hodograms at increasing times, starting from $t = 30\ \Omega^{-1}$, in steps of $30\ \Omega^{-1}$, each interval averaged over $20\ \Omega^{-1}$ (see section 2 for the reasoning behind the averaging). Each hodogram shows the transverse field components between $\pm 1.2\ B_0$. Thus, the upstream point is, as throughout the paper, at the right side ($B_z = B_0 \cos\theta_{Bn} > 0$, $B_y = 0$). The dashed lines in the first panel (top left) indicate that the rotation angle $\alpha$ has a finite deviation from 180°. The series of hodograms clearly shows that although in this case at first an electron sense rotation forms, the RD eventually reverts to the minimum shear, ion sense solution. The electron sense rotation is shed upstream as a damped, solitary wave (cf., *Krauss-Varban* [1993]) that soon dissipates in this relatively high-beta plasma. By $t = 300\ \Omega^{-1}$, the hodogram looks identical to the last interval displayed here except that there is no significant trace of the upstream rotation left. The timescale for complete formation of the ion sense RD can vary from a few $\Omega^{-1}$ to $\sim 100\ \Omega^{-1}$, depending on $\beta_i$, $\theta_{Bn}$ and $\alpha$. Some ion sense RD's do not start with a discernible electron sense rotation at early times. The main point here is that even when the deviation from coplanarity is quite small, we obtain the minimum shear solution (most direct rotation), in agreement with previous results at multiple discontinuities [*Omidi*, 1991] and for ISs [*Karimabadi and Omidi*, 1992; paper 1], as well as observations.

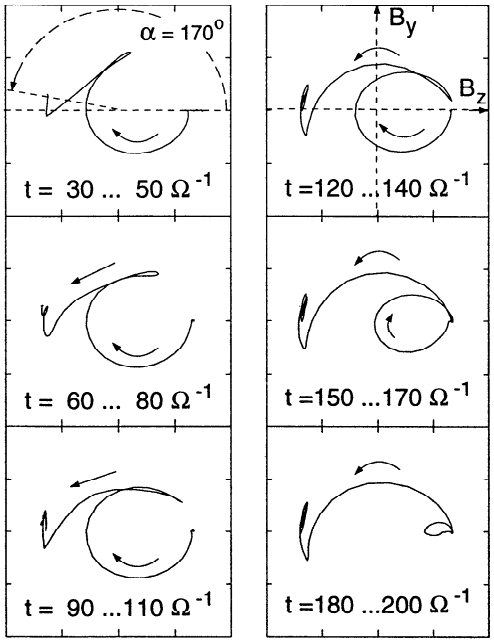


**Figure 4.** Evolution of a noncoplanar ion sense RD (rotation angle $\alpha = 170°$, $\theta_{Bn} = 60°$, and $\beta_i = 1$) from an initial electron senselike hodogram to the minimum shear solution. Here and in all other hodograms the vertical axis is $B_y$, the horizontal is $B_z$, and the range plotted is $\pm 1.2$ of the upstream magnetic field $B_0$. The plots of the fields are averaged over times as indicated, where $\Omega$ is the ion cyclotron frequency. Arrows indicate sense of rotation; all RDs start with $B_y = 0$ and $B_z = B_0 \sin\theta_{Bn}$ upstream.

**Hodograms and wave trains.** Figure 5 shows a series of hodograms for rotation angles $\alpha = \pm 90°$, $\pm 160°$, $\pm 170°$, and $\pm 180°$ at $\theta_{Bn} = 80°$ and $\beta_i = 1$ towards the end of each simulation. Quite obviously

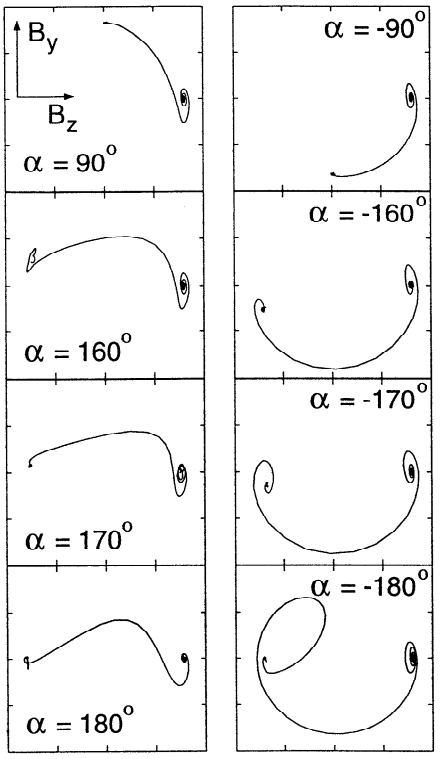


**Figure 5.** Comparison of noncoplanar and coplanar ion sense rotations (left column) and electron sense rotation (right column) for rotation angles $\alpha$ as indicated and $\theta_{Bn} = 80°$, $\beta_i = 1$. Note that here all cases have an upstream wave train.

in each case the minimum shear solution has formed. Although there are some changes with $\alpha$, the solutions connect smoothly to the coplanar case. Note that both senses of rotation have a similar upstream wave train. It is right-hand elliptically polarized, mostly out of the **B**-**k** plane (**k**: wave vector, oblique propagation), and thus on the Alfvén/ion-cyclotron (A/IC) branch [*Krauss-Varban et al.,* 1994]. Such wave trains are an integral part of the RD structure and not caused by dispersive broadening of the RD [*Krauss-Varban,* 1993]. They are related to the internal current structure of the RD, that is, the relative excursion between the transverse ion velocity and the transverse magnetic field. The associated current is responsible for the upstream hooks (reverse rotation) and downstream overshoots of the hodograms. When the conditions are right, that is, sufficient upstream or downstream directed group velocity and sufficiently low damping, the same current also produces a nearly phase-standing wave train (see section 4 below).

Note that the existence of a wave train is independent of the RD's sense of rotation. The wave trains are always on the A/IC branch of kinetic theory due to the proximity of the normal component of its group velocity $v_{gx} = |\mathbf{v}\cdot\mathbf{n}|$ and phase velocity $v_{ph}$ to $v_{An} = v_A \cos\theta_{Bn}$. They are always right-handed here because we chose the magnetic field to point downstream, and the polarization of the A/IC mode is right-handed at sufficient propagation angle and beta [*Krauss-Varban et al.,* 1994].

The RDs' velocities are often slightly smaller than $v_{An}$ due to the existence of back-streaming ions (typically $\lesssim 4\%$ for coplanar RDs). This effect is much smaller than at strong ISs and has little consequence on wave propagation. More importantly, for the local plasma condition the kinetic solution for $v_{ph}$ and $v_{gx}$ is significantly different from the dispersion that is anticipated from Hall-MHD [*Krauss-Varban et al.,* 1994]. Since several conditions have to be satisfied for such waves to exist (concerning the size of $v_{gx}$ and the damping at wavelengths of the order of the RD gradient scale, see section 4) it is not surprising that they are not always present. Using linear theory we have confirmed that their presence and wavelength are consistent with the measured gradient scale (wavenumber $k = \mathcal{O}(1/\ell)$ ) and actual RD propagation speed. In section 4 we explain the behavior of upstream and downstream wave trains as a function of $\beta_i$ and $\theta_{Bn}$ in more detail.

Some hodogram features in Figure 5 change when $\alpha$ becomes close to 180°. For example, the well-known overshoot of the electron sense rotations [*Goodrich and Cargill,* 1991] only develops in the vicinity of 180°. In other words, in most cases no large overshoot should be observed. A typical characteristic of ion sense RDs is that they become quite flat close to $\alpha = 180°$. However, below we show that the flatness is a function of the ion beta and is not as pronounced at high $\beta_i$.

**Variation with $\alpha$.** Generally, we find that there is no significant qualitative variation of the solutions as a function of the rotation angle. All RDs have some reflected ions (see also *Swift and Lee* [1983]) and may have a slight downstream anisotropy ($T_{i\perp}/T_{i\parallel} > 1$). However, we find that the number of reflected ions, the deviation from the MHD RD speed $v_{An}$, any downstream anisotropy, and the internal plasma signatures become weaker with $|\alpha|$ away from 180°. For example, at $\theta_{Bn} = 80°$ and $\beta_i = 1$ the normalized density variation $|\Delta n|/n$ within the RD reduces from $\sim 50\%$ at $|\alpha| \sim 180°$ to $\sim 17\%$ at $|\alpha| \sim 90°$. This is to be expected because for $|\alpha| \longrightarrow 0$ all plasma perturbations should vanish. Consistent with these characteristics, any upstream or downstream wave train (if existent) also becomes weaker.

**Stability and nonexistent jumps.** To show the stability of the RD solution over time and the fact that there are indeed no jumps in the plasma quantities, we present one example in more detail. Figure 6 shows stack plots of the two transverse magnetic field components over 50 $c/\omega_p$ in the vicinity of the RD, and for the last 400 $\Omega^{-1}$ of the simulation. This RD has an electron sense rotation $\alpha = -90°$ with $\theta_{Bn} = 80°$ and $\beta_i = 1$. Also shown are the magnetic field, density and ion temperature profiles (normalized with their respective upstream values) over a 200 $c/\omega_p$ region towards the end of the simulation ($t = 500$ to 700 $\Omega^{-1}$; see section 2 for an explanation of the averaging). It is clear that there is no evolution of the RD over these timescales and that there are indeed no significant changes of the plasma quantities across it. Close to the right-hand wall one can see minute changes of $B$ and $T_i$ of the order of

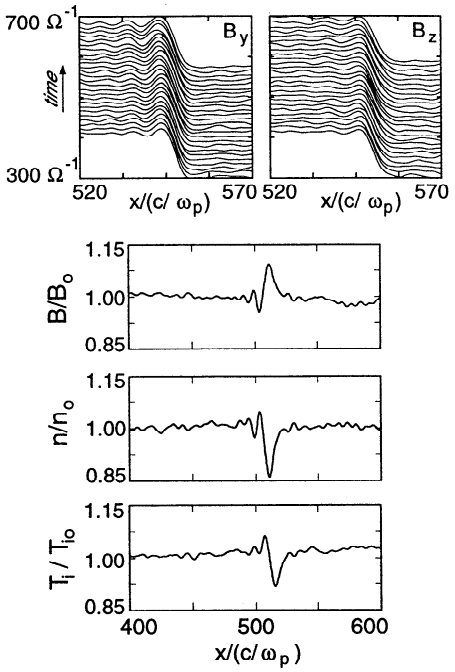


**Figure 6.** Example of a noncoplanar electron sense RD, with $\theta_{Bn} = 80°$, $\alpha = -90°$, and $\beta_i = 1$. The top side-by-side stack plots show the profile of the transverse magnetic field components over a region of 50 ion inertial lengths $c/\omega_p$ around the RD as a function of time. The plots of the magnetic field $B$, density $n$ and ion temperature $T_i$ are all normalized with their respective upstream value and are over a region of 200 $c/\omega_p$ around the RD. Note that there is no upstream to downstream change of the plasma quantities and that the RD is basically stationary.

1 to 2%, which are due to perturbations from the initial formation of the RD. Over time the RD propagates away from this slightly perturbed plasma. The amplitude and spatial extent of such perturbations vary from case to case, but (after sufficient time to allow the RD to propagate out and "decouple from the piston") can always be distinguished from actual jumps associated with an IS. We also performed a limited number of simulations that included upstream perturbations (of the order of 5 to 20%) and flow speed changes. In all cases we found that the discontinuity remained an RD.

**Time-dependent intermediate shock.** As shown in paper 1, both noncoplanar weak and strong ISs can exist in a collisionless plasma, and evolve over a timescale of typically many 100 $\Omega^{-1}$ into RDs, that is, the jumps become weaker over time and the internal signatures of the plasma quantities become identical to those of RDs. During this evolution the original thickness of the rotational layer is maintained. For the weak ISs this is the same as that of the corresponding RD solutions obtained from the piston method. In other words, although the noncoplanarity demands that the IS must be time-dependent, this does not necessitate that the main current layer broadens over time. Weak ISs do not always form if $|\alpha|$ is sufficiently away from 180°. Figure 7a shows the attempt to create an IS for

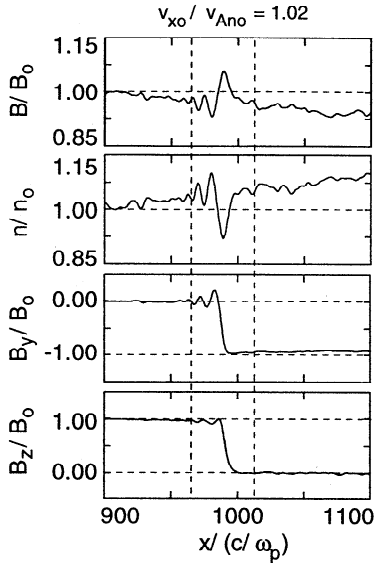


**Figure 7a.** Attempt to form a weak time-dependent IS (TDIS) for parameters as in Figure 6 and Alfvén Mach number $v_{xo}/v_{An} = 1.02$. Contrary to less noncoplanar TDISs (e.g., $\alpha = 160°$, see paper 1), here no TDIS forms. There is no jump of $B$ or $n$ over the region that contains the rotation and the internal plasma signatures (dashed lines). The normalized $B$, $n$, and transverse field components are shown over a region of 200 $c/\omega_p$ at the end of the simulation.

the same parameters as the RD in Figure 6 ($\alpha = -90°$). The Alfvén Mach number is $v_{xo}/v_{Ano} = 1.02$ which is roughly 2/3 from the RD limit to the highest Mach number IS. The (coplanar) Rankine-Hugoniot conditions predict a jump of 9% in the density, and 15% in both the temperature and magnetic field. Figure 7a shows the normalized magnetic field, density, and magnetic field components towards the end of the simulation ($t$ = 700 to 900 $\Omega^{-1}$). The magnetic field and density profiles are very similar to that of the RD, with a weak upstream wave train. The dashed lines indicate that over a reasonable region around the current layer there are no changes in $B$ or $n$. The ramplike shape of these two quantities is solely caused by the fact that there are now counter-streaming ions that, if they were to couple, would form the shock. However, this is not the case. Figure 7b shows the perpendicular ion tem-

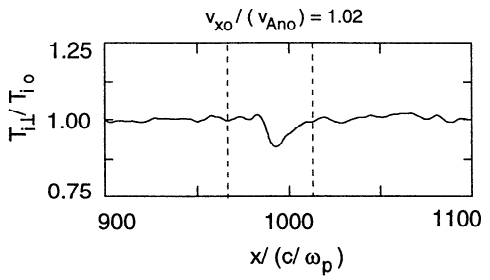


**Figure 7b.** Perpendicular ion temperature $T_{i\perp}$ normalized with its upstream value for the same simulation as in Figure 7a. Dashed lines indicate same regions as in Figure 7a. There is no temperature jump across the rotational layer nor within the wider area of 200 $c/\omega_p$ around the discontinuity.

perature in a similar format. It is clear that not only through the rotational layer, but also in general there is no heating associated with the structure. Figure 7c shows the upstream and downstream parallel velocity distribution function, evaluated over regions as indicated in the top panel. Again, it is clear that the two are basically identical, and no dissipation has taken place. Thus, in some cases of noncoplanar weak ISs there is not sufficient dissipation, such that the IS evolves into an RD very quickly, or never quite forms. In paper 1 we have shown that the corresponding strong (noncoplanar) intermediate shock does maintain itself for a much longer time. Similarly, when $|\alpha|$ is closer to 180°, the IS stays longer. In other words, the timescale for the evolution of noncoplanar ISs is a function of parameters, but such that there is apparently more effective dissipation closer to 180° and for the strong versus weak IS. Close to $|\alpha| \sim 180°$ the IS may remain for a sufficiently long period of time to be relevant for the open magnetopause. Figures 7a–7c serve as an example to demonstrate that with sufficiently careful simulations, RDs, ISs and time-dependent ISs can clearly be distinguished, even though the total jumps of weak IS are small for magnetopause parameters.

### 3.2. Coplanar Rotations

Although a magnetic field rotation of 180° could be disregarded as an unimportant singular case, it presents a special situation in that it allows a time stationary intermediate shock solution from the MHD viewpoint. *Wu* [1988] first proposed the existence of weak and strong ISs based on resistive MHD calculations. Subsequent kinetic simulations have supported the existence of ISs [*Wu and Hada,* 1991a; *Karimabadi and Omidi,* 1992]. *Wu and Hada* [1991b] also suggested that coplanar RDs would be unstable and develop into ISs. However, hybrid simulations with small or negligible resistivity demonstrated the existence of kinetic coplanar RDs [*Lee et al.,* 1989; *Goodrich and Cargill,* 1991; *Krauss-Varban,* 1993]. It is of interest to investigate the width and structure under typical magnetopause conditions without predetermining the thickness, by using the piston method. At the same time the relation to weak ISs becomes clearer. As we show here and in section 4, there are some major differences between ion sense and electron sense rotations.

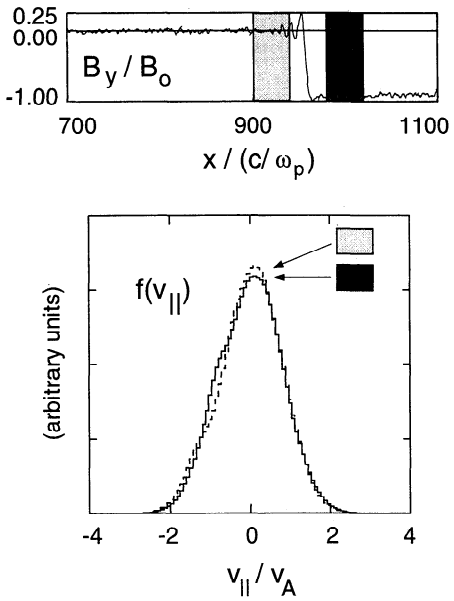


**Figure 7c.** Ion density distribution $f(v_{i\|})$ as function of the parallel velocity normalized by the Alfvén velocity for same simulation as in Figsures 7a and 7b. Solid line: averaged over upstream region indicated by light shading in graph of $y$ component of $B$ on top; dashed line: averaged over downstream region indicated by dark shading in graph on top. There is no significant change of the ion distribution across the rotation.

**Electron sense.** Going towards $|\alpha| = 180°$ we find in our simulations a general increase in the number of reflected ions, and also in the amplitude of initial perturbations. For that reason, these simulations typically have to be run longer before a clear asymptotic downstream state is reached (see example below). This alone hints at the fact that a neighboring state with finite dissipation does exist.

Figure 8 shows the normalized magnetic field, density profiles, and hodograms for three coplanar electron sense RDs with different $\theta_{Bn}$ and $\beta_i$, as indicated. In each case 75 $c/\omega_p$ of the total box (600, 700, and 700 $c/\omega_p$) are shown. The hodograms are for the same $x$ interval, as before displaying the transverse field components between $\pm 1.2\ B_o$. Each case shows time-averaged values ($t$ = 400 to 600, 600 to 800, and 600 to 800 $\Omega^{-1}$). The vertical dashed line indicates where the $z$ component of the magnetic field goes through zero (for the first time).

Several conclusions can be drawn from the results. First, as in the case of noncoplanar rotations, a wave train may form either upstream or downstream or may be absent. Also, from these and additional simulations we find that in general the amplitude of wave trains decreases with $\beta_i$. As a result, the hodogram becomes simpler in Figure 8. This contrasts to solar wind RDs, which typically have a wide range of $\theta_{Bn}$ and $\beta_i \lesssim 1.0$. Thus if sufficiently thin, solar wind RDs should have a greater variation of hodograms and more pronounced wave trains.

Note that the density and magnetic field are nearly everywhere anticorrelated in Figure 8. An exception is the initial decrease of $B$ in the small $\theta_{Bn}$ current layer. The excursion of the transverse magnetic field becomes successively larger with both $\theta_{Bn}$ and $\beta_i$. The same scaling with $\beta_i$ is also seen in the ion sense rotations (Figure 12). Figure 9 shows (for $\theta_{Bn} = 60°$ and $\beta_i = 1.0$) that the ion temperature and anisotropy $T_{i\perp}/T_{i\|}$ are in phase; careful inspection shows that they are also in phase with the density plotted in Figure 8. This is also true for the internal structure of the other two cases (not shown). Also, the main signatures (except for a finite jump) are nearly identical to the example of an IS shown in Figures 4f–4j of paper 1, for the same plasma parameters. Apart from the overshoot,

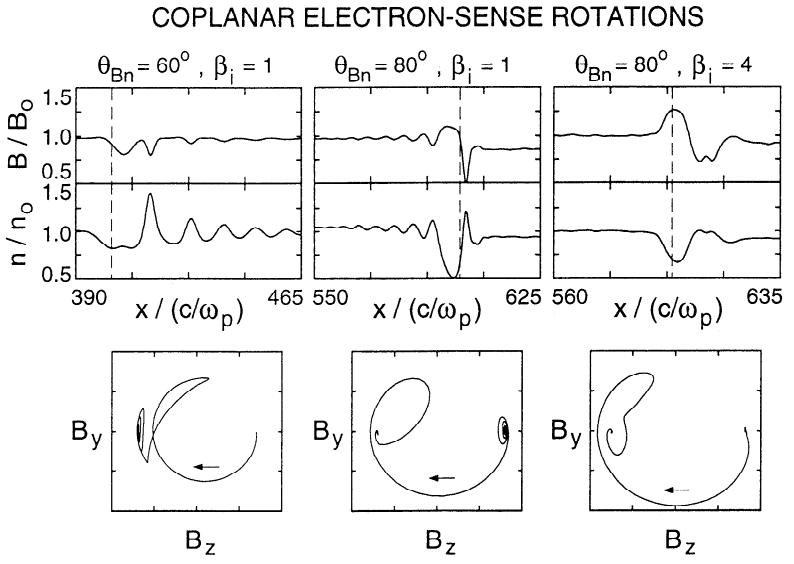


**Figure 8.** Normalized density $n$, magnetic field $B$ profiles and hodograms of three coplanar electron sense RDs with upstream parameters as indicated. Dashed lines indicate location where $B_z$ has its (first) zero (center of magnetic field rotation). The spatial region shown encompasses 75 $c/\omega_p$ in all cases, also for hodograms. Note that the wave train may be downstream, upstream, or nonexistent.

downstream oscillations are nearly invisible in $B_z$, that is, they are nearly linearly polarized and in the component out of the $\mathbf{B_o}, \mathbf{k}$ plane, as expected from oblique A/IC waves. Figure 9 is also typical in that it shows a slight average anisotropy $T_{i\perp}/T_{i\|} > 1$ downstream and the opposite anisotropy upstream, due to reflected

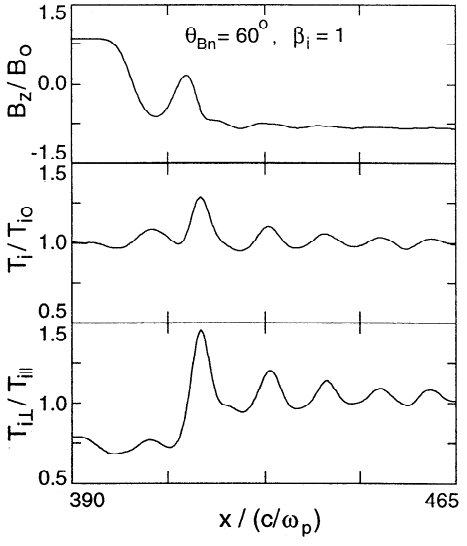


**Figure 9.** Example of a coplanar electron sense RD, with parameters as indicated. The plots of the $z$ component of the magnetic field $B_z$ and ion temperature $T_i$ are normalized with their respective upstream value. All curves, including the ion temperature anisotropy $T_{i\perp}/T_{i\|}$, are over the same region of 75 $c/\omega_p$ as in Figure 8. $T_i$ and $T_{i\perp}/T_{i\|}$ are correlated with $n$ in Figure 8 and anticorrelated with $B$. Note that there is no upstream to downstream jump of the plasma quantities. The upstream anisotropy is caused by backstreaming ions.

ions. The density of reflected ions at oblique, coplanar RDs is typically $\lesssim 2-4\,\%$ and thus comparable to that at weak ISs, but significantly smaller than for strong ISs (paper 1). The latter also have sufficient heating that upstream leakage of downstream ions plays a role, which is not the case here. Generally, we find the density of reflected ions to decrease with $\beta_i$, $\theta_{Bn}$, and $|\alpha|$. Note that the reflection takes place at the field rotation and is independent of the piston method used here; thin RDs formed with the nondynamic method also show reflected ions (see, e.g., work by *Krauss-Varban* [1993]). Typically, there is a larger reflected ion density at the beginning of the simulation, with an asymptotic decrease to $\lesssim 2$–$4\,\%$ towards the end of the simulation.

From Figure 9 it is clear that there is no heating associated with the field rotation. Similar to the noncoplanar rotations, there is no permanent change of the magnetic field or density across the rotation. However, for an angle of $\theta_{Bn} = 80°$ the RDs move very slowly in the simulation. Thus it takes a very long time for the RDs to decouple from the right-hand wall and from initial perturbations that are a consequence of the boundary condition (initial field rotation within one simulation cell). This is apparent in Figure 8, which shows that the asymptotic state is not quite reached yet for $\theta_{Bn} = 80°$. However, the value of the downstream magnetic field plotted over time in Figure 10 (for $\beta_i = 1$) demonstrates that the configuration is evolving into a true RD. A similar but faster evolution is found for $\beta_i = 4$ (not shown). It is interesting that this problem of a relatively long decoupling time (before the rotation can be identified as an RD) occurs only in the coplanar case, for which IS solutions also exist, but not in the noncoplanar case, for which we find that weak TDISs either do not exist or evolve into RDs (see paper 1 and section 3.1 above). The plasma in the perturbed (but

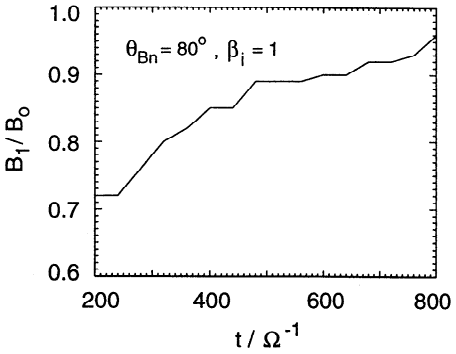


**Figure 10.** The downstream of the RD may be initially perturbed. Shown here is the course of the downstream to upstream $B$ field ratio over time for the case $\theta_{Bn} = 80°$ and $\beta_i = 1.0$ shown in Figure 8. In some cases as in this one the full decoupling from the piston may take several hundred inverse ion-cyclotron frequencies $\Omega^{-1}$. Contrary to MHD expectation (Figure 3) and our kinetic findings (paper 1) for ISs, there is no temperature jump here, and $n$ is actually slightly below $n_o$ at early times (see Figure 8), indicating a transient feature that is not related to an IS.

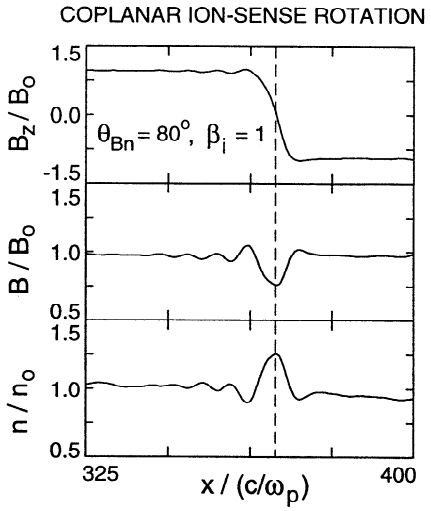


**Figure 11.** Example of a coplanar ion sense RD, with parameters as indicated. Plots of the normalized $z$ component of the magnetic field, the total magnetic field $B$, and the density $n$ over a region of 75 $c/\omega_p$ around the RD. Dashed line indicates location where $B_z$ has its (first) zero (center of magnetic field rotation). Note that there is no upstream to downstream change of the plasma quantities.

nonpropagating) area close to the right-hand boundary has a temperature anisotropy $T_{i\perp}/T_{i\parallel} \sim 1.2$ to 1.4. While the initial downstream values of both the magnetic field and the density are perturbed (Figure 8), there is no compression here. The density is actually lower than upstream, contrary to the Rankine-Hugoniot solution (see section 2) for an IS or our actual findings for collisionless ISs (paper 1). This confirms that the perturbed downstream area is simply a transient of the RD formation at large $\theta_{Bn}$ and that there is not a temporary formation of an IS.

**Ion sense.** For the limit $\alpha = 180°$, without exception electron sense rotations form, that is, they appear to be preferred. However, when the boundary value is defined via the vector potential (identical to setting the electric field), ion sense rotations result for $\alpha = 180°$. Thus, we find that both senses are allowed solutions in the coplanar limit. Which sense of rotation forms depends on which quantity (the electric or magnetic field) can freely float at the boundary, but that question is secondary here. The same choice of boundary conditions determines electron versus ion sense weak ISs (paper 1).

Figure 11 shows an example of a coplanar ion sense rotation for $\theta_{Bn} = 80°$ and $\beta_i = 1.0$. As for the electron sense, there is only a weak wave train. The downstream values of $B$ and $n$ have approximately reached the expected (i.e., upstream) level, albeit the density is still slightly disturbed from the initialization and slightly below $n_o$. Figure 12 shows the hodogram for this case and two other values of the ion beta, as indicated. Apart from the somewhat elliptical polarization of the last cycle of the wave train, the field rotation is flat, but clearly left-handed. As for the electron sense rotations, the excursion of the transverse field increases with $\beta_i$ such that the hodogram eventually looses its flat appearance that is otherwise typical (in solar wind observations as well as in hybrid simulations [*Neugebauer,* 1989; *Goodrich and Cargill,* 1991]). Note also that the upstream wave train has vanished at $\beta_i = 4$ but instead a downstream overshoot has developed. This shows the extreme variability of details of the hodogram as a function of pa-

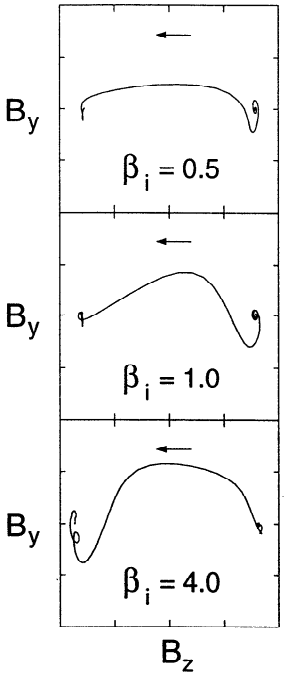


**Figure 12.** Hodograms of coplanar ion sense rotations for $\theta_{Bn} = 80°$ and increasing ion beta, as indicated. Arrow indicates sense of rotation. Note that RD becomes successively less flat for increasing $\beta_i$, and that the details of the hodogram change considerably with $\beta_i$.

rameters. The parameter-dependence of the internal signatures and wave trains is discussed in more detail in the next section.

## 4. Discussion

### 4.1. Internal Structure and Comparison With Generalized Fluid Theory

Whether the magnetic field, density, and temperature increase or decrease within the RD layer is generally not only a function of the sense of rotation but also of $\beta$, $\alpha$, $\theta_{Bn}$, and the location within the current layer. However, for high $\beta_i$ and RDs with small magnetic field normal component we find consistently that at ion sense rotations the density and ion temperature increase within the current layer and the magnetic field decreases, and vice versa at electron sense rotations. There is also an ion temperature anisotropy $T_{i\perp}/T_{i\|} > 1$ within the current layer that is much stronger for ion sense rotations than for the electron sense, and is correlated with the density perturbation. The above statements exclude the field signatures in wave trains and overshoots (compare also the hodograms in Figure 8). In the overshoots of electron sense RDs the total magnetic field actually decreases, and the density, temperature, and ion anisotropy $T_{i\perp}/T_{i\|}$ increase similar to the internal structure of ion sense RDs. The perturbations of the ion temperature and anisotropy are typically larger in the overshoot than throughout the main field rotation of electron sense RDs.

It is of interest to see to what extent these signatures can be described by a generalized fluid theory. Such a comparison is useful because it sheds light on the physical processes responsible for the internal structure. For this purpose we have developed a generalized fluid theory of RDs, which is described in detail in the Appendix. The theory assumes stationarity and expands the generalized fluid equations to first order around the nonlinear RD solution of ideal MHD. The calculation proceeds via the momentum and pressure equations and results in a coupled set of equations for the magnetic field and density signatures $\Delta B$ and $\Delta n$. The equations are closed either through adiabatic assumptions from theoretical considerations or, as done here, by using appropriate equations-of-state derived from the simulations. The theory provides the internal plasma signatures (i.e., deviations from ideal MHD) as a linear function of the local rate of rotation $\epsilon = \alpha' c/\omega_p$, measured in ion inertial lengths, which also can be viewed as the smallness parameter. The rate of rotation may be assumed to be some smooth function of $x$ with specific thickness (larger than the kinetic scales), or local values of $\alpha'$ from the hybrid simulations may be substituted for direct comparison. The calculated perturbations change sign with $\epsilon$, and the theory does not give a particular length scale. We would like to note in passing that this theory can also be employed as a diagnostic aid on spacecraft data to help interpret certain kinetic effects and filter out those perturbations directly associated with rotational structures from other, say, compressional waves.

As discussed in the Appendix, a Hall-MHD model gives incorrect signatures for finite $\beta_i$. Also the CGL double-adiabatic theory [*Chew et al.*, 1956] cannot properly describe the internal perturbation, because it assumes zero heat flux and magnetic moment conservation, which are both inconsistent with the kinetic simulation results. We therefore use an adapted fluid theory in which the parallel and perpendicular polytropic coefficients are matched to our findings of correlation between $n$ and $T_{i\perp}$ and $T_{i\|} \sim$ const, that is, $\gamma_\perp = 2$ and $\gamma_\| = 1$. Including anisotropy perturbations and using realistic equations of state yields the correct sign of the $B$ perturbation and gives a resonable dependence on $\beta_i$.

The results for four cases are shown in Figure 13. The plasma and RD parameters are as indicated. The top

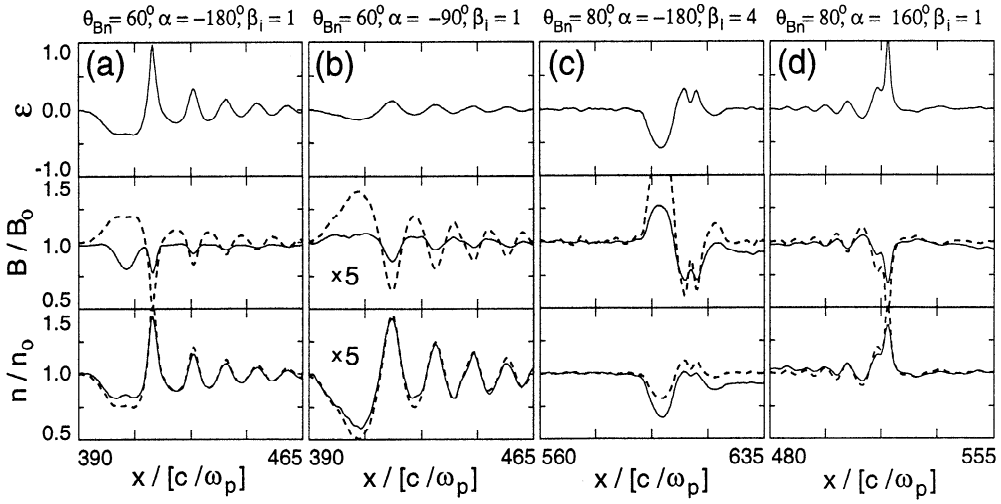


**Figure 13.** Comparison of hybrid simulation results (solid lines) to internal signatures predicted by a generalized fluid theory (dashed lines), using the local rate of rotation $\epsilon$ from the simulation as displayed in the top panels. The center and bottom panels show the normalized magnetic field and density, respectively, for four RDs with plasma parameters as indicated, over a range of $75c/\omega_p$ around the RD.

panels show $\epsilon$, the center panels show the normalized magnetic field, and the bottom panels show the normalized density for a region of $75c/\omega_p$ around the RD. The solid lines indicate the hybrid results, the dashed lines are from the generalized fluid theory, using the local $\epsilon(x)$ as input and ignoring FLR corrections. While $n$ is generally well-described by the fluid theory, the $B$ perturbation is typically a factor of two to three too large. Since the fluid theory retains anisotropy effects and we matched the polytropic coefficients, the temperature components and total temperature (not shown) are described with the same accuracy as $n$. With a few exceptions, both the structure of the internal layer and the wave train show similar agreement. As discussed in the Appendix, neglecting FLR effects consistently overestimates $|\Delta B|$. Since the well-known CGL-FLR terms are inappropriate, new, adapted terms would have to be calculated to improve the fluid theory.

Figure 13a shows a case ($\theta_{Bn} = 60°$) where the perturbations $\Delta B$ and $\Delta n$ in the layer are correlated for the electron sense rotation, contrary to the general oblique and high $\beta$ behavior. Comparison with Figure 9 shows that this is the region where significant ion reflection occurs, leading to a large $T_{\|}$. To test the hypothesis that this signature is caused by the ion reflection process, we show in Figure 13b the same case except for a rotation angle of only $-90°$, where we usually see much less ion reflection. Here all signatures are much smaller (scale factor of five applied). The results show that now $\Delta B$ and $\Delta n$ are correlated, suggesting that ion reflection can play a major part in the internal signatures, and can cause the $\Delta B$ to be negative for both ion and electron sense rotations.

Figure 13c shows one of the cases where (at the time displayed) the asymptotic downstream $n = n_0$ is not quite reached. As mentioned in the previous section, there is some downstream anisotropy associated with this effect. The mismatch to the generalized fluid results suggests that these finite jumps of the anisotropy, $B$, and $n$ start at the outset of the field rotation. Finally, Figure 13d shows that there is a similar degree of resemblance between the fluid and hybrid results also for an ion sense rotation, and the case of an upstream wave train.

The top panels indicate that $\epsilon$ varies from $\ll 1$ to $\sim 1$. A look at $n$ proves that the analytical theory is quite robust and gives reasonable results although $\epsilon \ll 1$ has been assumed. In other words, the fact that $\epsilon$ may approach unity is not the reason for the discrepancies between fluid and hybrid results. To conclude, all the various kinetic effects including finite heat flux and ion reflection play part in creating the internal signatures of RDs.

### 4.2. Scale Sizes

Comparing the magnetic field gradient scales (half widths) to those obtained with the nondynamic method (all at $\theta_{Bn} = 60°$, *Krauss-Varban* [1993]), we find that the dynamic method used in this work gives the same results as the minimum scale that can be obtained when the RD is (carefully) initialized with a given width at the beginning of the simulation (nondynamic method). As before we find that the total width of the structure (region over which the magnetic field and the density are perturbed, excluding wave trains) scales with the ion inertial scale and the ion gyroradius $\rho_{Li}$, also at $\theta_{Bn} = 80°$. The total thickness is at least four times as large as the gradient scale, but can be up to ten times as large. For example, at $\theta_{Bn} = 80°$ we find the total width to be about 10 to 15 $c/\omega_p$ at $\beta_i = 0.5$; it increases to about 25 to 35 $c/\omega_p$ at $\beta_i = 4.0$, for both electron and ion sense rotations. The gradient half width is actually quite similar for the whole parameter region studied here, $1 \lesssim \ell/(c/\omega_p) \lesssim 3 - 4$. We find that for a small normal component of $B$ ($\theta_{Bn} = 80°$) $\ell$ no longer simply scales with the upstream $\rho_{Li}/(c/\omega_p) = (\beta_i)^{1/2}$ or $1 + (\beta_i)^{1/2}$. Figure 14 shows the evaluated gradient scale for the three electron sense RDs of Figure 8. For $\theta_{Bn} = 60°$ the thickness is relatively large and agrees with the minimum thickness found in our previous simulations (nondynamic setup). Note that there is always a finite evolution time before the gradient of the RD is well-defined. For $\theta_{Bn} = 80°$, the internal scale is no longer a function of the upstream $\beta_i$, and $\ell$ is of order unity. Whether such thin current layers may be unstable to perturbations perpendicular to the normal direction can only be addressed with two-dimensional simulations.

Figure 15 shows the evaluated gradient scale as a function of $\beta_i$ for both senses of rotation and $\theta_{Bn} = 80°$. The ion sense RD's thickness still increases with $\beta_i$ until about $\beta_i = 2$, and then remains approximately

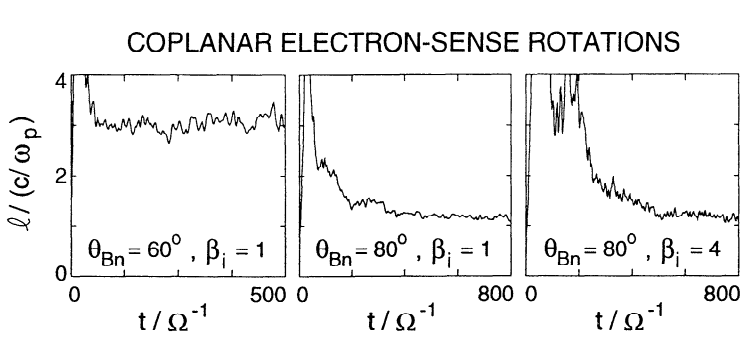


**Figure 14.** Gradient length scale (half width) $\ell$ normalized with the ion inertial length measured over time for the three coplanar electron sense RDs shown in Figure 8. These RDs are thinner for $\theta_{Bn} = 80°$ than for 60°, and $\ell$ does not increase with $\beta_i$.

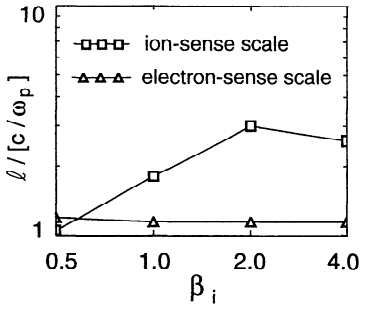


**Figure 15.** Gradient length scale (half width) $\ell$ as a function of $\beta_i$ for coplanar electron sense (triangles) and ion sense (squares) RDs at $\theta_{Bn} = 80°$. While $\ell$ increases initially with $\beta_i$ for the ion sense it ceases to do so for larger $\beta_i$.

constant. We have made additional runs at $\beta_i = 6$ and 8 and found approximately the same width $\ell \sim 3$. However, for such high values of $\beta_i$ and narrow RDs, the back-streaming ions generate A/IC waves similar to those at some ISs (compare paper 1) and slow shocks [*Omidi and Winske,* 1992]. These interfere with the RD such that the momentary thickness varies, around an average thickness of $\ell \sim 3c/\omega_p$. Note that for typical magnetopause parameters, the ion sense $\ell$ is about a factor of three larger than that of the electron sense.

The fact that the internal gradient width can be significantly shorter than the overall thickness, and may not always scale with the ion gyroradius, is not surprising if the RD is viewed as the IS limit. Kinetic work on shocks and observations have shown in the past that there may be multiple scales associated with collisionless shocks. For example, supercritical fast mode shocks have a foot that scales with the (convected) gyroradius, and a ramp that scales with the ion inertial length or may have substructure on electron scales (e.g., *Goodrich* [1985] and references therein). Here it appears that a small magnetic field normal component is decisive for the existence of thin ($\ell < \rho_{Li}$) current layers.

The arguments provided in the Appendix suggest that one of the reasons for the asymmetry between the ion and electron sense width is that the limiting factor (for finite $\beta_i$) is not the upstream $\beta_i$ or ion gyroradius $\rho_{Lio}$. Instead, given the finite perturbations of $T_{i\perp}$ and $B$, the local $\rho_{Li}$ should be considered. The dependence of the sign of $\Delta\rho_{Li}$ on the direction of rotation can help explain the apparent asymmetry of the width. According to (A16), at ion sense RDs the internal $\rho_{Li}$ is elevated, whereas it is reduced for electron sense RDs. This is in agreement with the simulations and also predicts that ion sense RDs should be slightly thicker than the upstream $\rho_{Li}$, whereas electron sense RDs should instead be limited by $c/\omega_p$. On the other hand, for less oblique propagation $\Delta\rho_{Li}$ is sufficiently small that it is again the upstream $\beta_i$ for both senses of rotation that limits the width. In addition, as discussed above, ion reflection can reduce the $\Delta B$ of the layer and thus destroy a perfect antisymmetry of the two senses of rotation.

To summarize, under typical magnetopause conditions the simulations predict two important differences between electron sense and ion sense rotations: one concerning the minimum gradient scale of the current layer (up to a factor of three thinner for electron sense rotations), and the other with respect to the sign of the internal signatures of the fields and moments ($n$ and $T$ up, $B$ down for ion sense; vice versa for electron sense).

### 4.3. Weak Intermediate Shocks and Uniqueness of Width

In paper 1 we found with the exception of electron sense strong ISs, that all ISs with typical magnetopause parameters have a thickness of the rotational layer that is commensurate with that of the RD in the corresponding weak IS limit. For $\theta_{Bn} = 80°$ and coplanar ISs, the rotational layer is also the region over which most of the dissipation occurs, roughly independent of the strength of the shock (see paper 1 for details). The essence of these results is that the type of solution that is formed depends on the amount of dissipation produced, which is not always sufficient to obtain the solution initially aimed for. Also, the total change in plasma quantities across weak ISs can easily be smaller than the internal signatures of the current layer. Superficially, such solutions look very much like RDs; their internal signature is (apart from the small jumps) basically identical.

In general, the thickness of RDs is not unique; they are different that way from shocks. The piston method selects a particular solution which we believe to be the one relevant to the magnetopause because of the dynamic formation. This width also happens to coincide with the minimum thickness that can be obtained by the nondynamic method. In addition, the piston method clarifies the relation to weak ISs. Another way of looking at this is to say that ISs have the Mach number as "free parameter," up to the RD limit. The coplanar RD should then have a thickness that corresponds to the scale of the coplanar IS. Away from $\pm 180°$ the RD has the rotation angle as "free parameter" and is no more bounded by a steady state IS. So, we find for example that the $\alpha = -180°$ RD at $\beta_i = 4$ is a factor of three thinner ($\ell \sim 1\ c/\omega_p$) than the corresponding RD at $\alpha = -90°$. But even for noncoplanar boundary conditions, RDs formed with the piston method can be viewed as the rotational part of a more general Riemann problem. Thus, they should be the ones relevant to the magnetopause. Indeed, their scale size is still in general agreement with the reported observed thickness of the magnetopause current layer.

### 4.4. Wave Trains

A curious finding is that depending on the parameters, there can be an upstream wave train or a downstream wave train, and sometimes there is none. This fact can actually be explained by the kinetic properties of the A/IC mode. In paper 1 we show an example of how the dispersion of the A/IC mode varies with wavenumber and propagation angle. While the A/IC mode always starts with a phase velocity of $v_{ph} = v_{An}$ at small wavenumbers $k$, it only has normal dispersion for sufficiently small propagation angle $\theta$ and $\beta_i$. For

typical wave train wavenumbers and intermediate $\beta_i$, the A/IC has normal dispersion at $\theta \lesssim 70°$ but attains anomalous dispersion at highly oblique propagation. The damping decreases with propagation angle, but increases with $k$ and $\beta_i$. Because the normal component of the group velocity remains at $\sim v_{An}$ before it changes when $k \sim \mathcal{O}(c/\omega_p)$, $v_{ph}$ is mostly still quite close to $v_{An}$.

Figure 16 shows several quantities as a function of $\theta_{Bn}$ and the ion beta $\beta_i$ (fixed $\beta_e = 0.2$). We have fixed the wavenumber to $k = 0.7\omega_p/c$, which is a medium value within the range of typical wavenumbers $k = 0.45$ to 0.85 found in the simulations. This range is a little smaller than the span of gradient scales $\ell \sim 1$ to 3 $c/\omega_p$ that we measured, presumably because the stronger damping at high wavenumbers will select the longer wavelength components of a wave train (which always has a finite spread in wavelengths). Although the dispersion and damping change with $k$, Figure 16 gives a reasonable qualitative picture of the A/IC mode properties.

The contour lines indicate the normal component of the group velocity normalized with the normal Alfvén velocity $v_{gx}/v_{An}$. Two contours each above (solid line) and below 1.0 (dashed line) are drawn. A value $v_{gx}/v_{An} > (<) 1$ indicates that any wave train, if existent, should be found upstream (downstream). The grey scale shows contours of the damping, measured as the ratio between the wavelength $\lambda$ to the spatial damping length

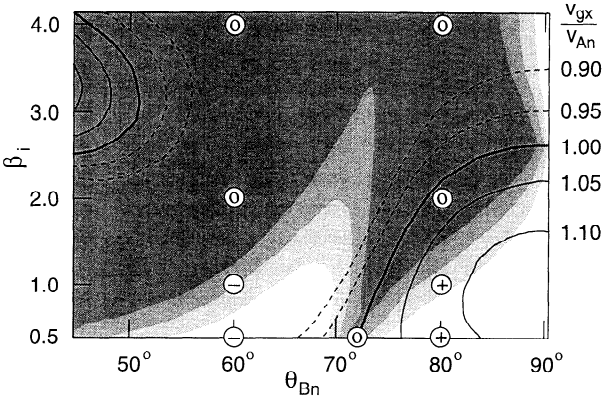


**Figure 16.** Contour plot of the Alfvén/ion-cyclotron (A/IC) group velocity $v_{gx}$ normalized with the normal Alfvén velocity $v_{An} = v_A \cos\theta_{Bn}$ and damping (grey scale) as a function of propagation angle $\theta = \theta_{Bn}$ and ion beta, for typical wave train wavenumber $k = 0.7\ \omega_p/c$. Contour levels as indicated, where a value $> 1$ ($< 1$) indicates upstream (downstream) directed group velocity in the frame of an ideal RD ($v_x = v_{An}$). Grey scale is a measure of damping (wavelength $\lambda$ divided by spatial damping length $\ell_\gamma = v_{gx}/|\gamma|$), with levels $\lambda/\ell_\gamma < 1$ (white), and $> 1$, $> 2$, and $> 3$ for successively darker shading. Circles with symbols indicate presence of downstream (minus), none (zero), or upstream (plus) wave trains in the simulations. The excellent agreement demonstrates that the mode properties of the kinetic A/IC mode explain the presence or absence and direction of a wave train.

$\ell_\gamma = v_{gx}/|\gamma|$, where $\gamma$ is the imaginary part of the complex wave frequency. White corresponds to $\lambda/\ell_\gamma < 1$, and the shaded areas correspond to successively larger damping, $\lambda/\ell_\gamma > 1$, $> 2$, and $> 3$, respectively. These levels can also be looked upon as where the wave amplitude drops by one e-folding within the time it takes for the wave energy to reach 1, 1/2, or 1/3 wavelengths distance from the RD. Actually seen damping may be a little smaller if the wavenumber is smaller than $0.7\ \omega_p/c$.

The circles show whether we found a downstream, none, or an upstream wave train in the simulations (minus, zero, and plus symbols, respectively). While Figure 16 is at a fixed wavenumber $k$, whereas the actual wavenumber found in the simulations varies, and the mode properties change somewhat with $k$, it is nevertheless evident that there is a good match between the simulation findings and the behavior expected from kinetic theory. Specifically, both linear kinetic theory and simulations predict that the wave train should be upstream and not downstream at large $\theta_{Bn}$. We have made an additional simulation run at $\theta_{Bn} = 72°$ as indicated in the Figure and found no wave train, as expected. Given that the gradient scale (and thus wave train wavelengths) is a rather weak function of $\beta_i$ (at most $\propto 1 + (\beta_i)^{1/2}$), whereas the damping is not, there should not be any wave trains at large $\beta_i$, in agreement with the simulation results. We should point out that while the amplitude may vary, the existence and direction of a wave train is not a function of $\alpha$ and independent of the sense of rotation (see, e.g., Figure 5). In other words, the graph clearly shows that the direction and presence of a wave train can be explained by the kinetic properties of the A/IC mode.

Wave trains at ISs are more difficult to predict for a variety of reasons (jumps in plasma parameters, reflected ions, upstream generated waves, and unsteady shock transitions). Also, some strong intermediate shocks have a significantly thicker shock transition and correspondingly larger wavelength of phase standing waves, which may then not be damped even at relatively large $\beta_i$. The same may apply to RDs or ISs with much smaller $\theta_{Bn}$ than considered here. Note that for very small $\beta_i$, the properties of the wave train change significantly with $\beta_e$ [*Vasques and Cargill,* 1993].

## 5. Summary and Conclusions

We have performed a large number of one-dimensional hybrid simulations to investigate the kinetic structure of the magnetopause field rotation. The kinetic structure of ISs was presented in paper 1 [*Karimabadi et al.,* this issue]. We demonstrated that internal signatures, the questions of existence and stability of RDs and ISs, and the associated dissipation can only be addressed with a kinetic approach. Using the piston method (dynamic method), we investigated typical magnetopause parameters (small magnetic field normal component, large ion beta) but restricted the study to the case of an isotropic plasma. Contrary to previous investigations of RDs in which the field rotation and thickness

had to be specified from the outset, in the dynamic method only the upstream and downstream boundary conditions are given, similar to what occurs at the magnetopause. While the previous investigations gave no unique scale size, and field rotations $|\alpha| > 180°$ were allowed, we found here that the piston method always gives a unique width of the RD, comparable to the smallest width obtainable with careful nondynamic formation, and always gives the minimum shear solution (smallest field rotation). Both of these findings are also valid for ISs (paper 1). Thus the minimum shear and unique thickness found in observed magnetopause crossing can be understood if the emergence of a rotational layer is viewed as a Riemann problem on kinetic scale lengths.

The region over which there are significant changes in $B$ and $n$ (excluding any wave trains) is typically 10 to 40 $c/\omega_p$ for RDs and weak ISs and is proportional to $(\beta_i)^{1/2}$. The gradient half width $\ell$ can be a factor of four to ten smaller, varies relatively little with parameters ($1 \lesssim \ell/(c/\omega_p) \lesssim 4$ for both RDs and weak ISs) and may be close to 1 $c/\omega_p$ even at high $\beta_i \sim 4$. The internal signatures and wave trains become smaller with the rotation angle $|\alpha|$, with little qualitative changes. Our simulations showed that depending on parameters, there can be upstream, downstream, or no wave trains associated with RDs. We explained the presence and direction of the wave train via the properties of the A/IC mode in kinetic theory.

The simulations gave a number of specific predictions concerning the kinetic structure of RDs for typical magnetopause conditions, which are with few exceptions also valid for weak ISs. There are significant differences between (oblique, high beta) ion sense and electron sense rotations. In the former the density and temperature increase in the current layer, and the magnetic field decreases. The opposite is the case for electron sense RDs. We developed a generalized fluid theory of RDs to aid in understanding which kinetic effects contribute to the internal structure. Comparison with the simulation results shows that CGL double-adiabatic equations of state [*Chew et al.*, 1956] are not satisfied. We find that finite ion inertia, anisotropic pressure perturbations, and FLR effects all contribute to the internal plasma signatures. There are also effects associated with reflected ions which the generalized fluid theory does not describe. At high $\beta_i$, electron sense RDs can be a factor of three thinner than ion sense RDs, which is at least partially a consequence of the size of the local ion gyroradius, whose deviation from the upstream carries a different sign for the two senses of rotation.

For typical magnetopause conditions, the jumps in the plasma quantities associated with an IS are quite small. We used a large number of macroparticles in the simulation and careful diagnostics to distinguish between RDs and ISs. We found that RDs exist and are stable for all parameters studied, that is, there is no discernible jump and no dissipation in the RD limit. Weak ISs, as studied in detail in paper 1, are very similar to their RD counterparts and have nearly identical internal signatures, wave trains, and widths. Since jumps for weak ISs for typical magnetopause conditions are very small, precise measurements of the plasma quantities ($B$, $n$, $T$) are required to identify a discontinuity observed at the magnetopause as weak IS. The largest jump would occur in the proper combination of these three parameters. Since the parallel temperature is difficult to define/measure in the presence of multiple, drifting ion components, the perpendicular ion beta $\beta_{i\perp}$ appears to be the most useful quantity. The change in $\beta_{i\perp}$ can be more than a factor of two even if the individual jumps are less than 20%. One has to keep in mind that temperature anisotropies will influence these results. Evidently, the irrefutable observation of local dissipation (beyond jumps due to anisotropy) would be a strong indication for the presence of an IS rather than an RD. For example, consistency between upstream-encountered plasma that is leaked from downstream and downstream-encountered plasma may indicate that observed dissipation is local and the discontinuity approximately one-dimensional (see also *Fuselier et al.* [1993]).

Ion reflection does not only occur at ISs but also at RDs. While the density of reflected ions is significantly smaller than at strong ISs, it is comparable to that at weak ISs ($\lesssim 2-4\%$). This means that without quantification, the mere presence of reflected ions in observations [*Sonnerup et al.*, 1981; *Gosling et al.*, 1990; *Fuselier et al.*, 1991; *Gosling et al.*, 1991] cannot be taken as a signature of an ISs. Moreover, in anisotropic plasmas ion reflection at RDs can be more significant [*Omidi*, 1991; *Karimabadi*, 1994].

Due to their larger jumps, strong ISs should be easier to identify. Both weak and strong IS can also exist as TDIS in the noncoplanar situation. While in general all three, weak and strong ISs and RDs, may be relevant to the magnetopause field rotation, weak TDISs have a relatively shorter evolution time to RDs ($\lesssim 100\ \Omega^{-1}$) or do not exist far away from coplanarity. The processes that lead to an open magnetopause are probably anything but stationary. It is of interest to see whether in the real world this time-dependent formation of rotational layers is more accurately approximated by ISs or by RDs. An obviously necessary theoretical generalization is to study the properties of these discontinuities in detail in anisotropic plasmas.

## Appendix: Generalized Fluid Theory of RDs

We outline a generalized, nondissipative fluid theory of RDs. The treatment gives useful insights into the scope of applicability of fluid theory and allows for direct comparisons with kinetic solutions. We first give a brief description of the approach, assumptions, and the analytical derivation. After that, the consequences of various models for the ion fluid are discussed.

Starting points are the one-dimensional steady state two-fluid equations without electron inertia and with

zero resistivity. Both ion inertia and finite Larmor radius (FLR) terms are retained in this formalism. Our approach is a first-order expansion about the (nonlinear) ideal MHD RD solution. In this way the calculation provides the internal signatures of RDs of finite thickness. All quantities $A(x)$ are written in terms of their upstream (i.e., unperturbed) value (subscript $o$) and a spatially varying perturbation: $A(x) = A_o + \Delta A(x)$.

We stress the fact that for consistency, the Hall term and the FLR effects can only be carried to first order. This can be seen as follows. Because of the relation $\rho_{Li} = (\beta_i)^{1/2}\, c/\omega_p$ for the ion Larmor radius, $\rho_{Li}$ and $c/\omega_p$ are of the same order for the range of of ion betas we are interested in (say, $1/4 \lesssim \beta_i \lesssim 4$). However, the FLR terms themselves are derived from an expansion of the kinetic equations in $\Omega^{-1}$ [*Macmahon,* 1965; *Chhajlani and Bhand,* 1980]. In our application the timescale condition $\tau \gg \Omega^{-1}$ is equivalent to $\ell \gg c/\omega_p$ or $\gg \rho_{Li}$, where the typical spatial scale is our gradient length $\ell$. As a consequence, a higher order calculation is inconsistent with the formulation of FLR theory. In other words, the first-order expansion presented here is complete as far as the use of standard FLR theory is concerned.

By using polar coordinates for the transverse magnetic field ${B_t}^2 = {B_y}^2 + {B_z}^2$, $B_y = B_t \sin\alpha$, $B_z = B_t \cos\alpha$, it can be seen that the smallness parameter

$$\epsilon = \alpha' c/\omega_p \tag{A1}$$

is the local rate of magnetic field rotation

$$\alpha' = \left(B_y' B_z - B_y B_z'\right) / {B_t}^2 \tag{A2}$$

measured in ion inertial lengths. In the above, the prime indicates the derivative with respect to the normal direction $x$. Note that except for the transverse components of the magnetic field and flow velocity $\mathbf{v}$, all derivatives vanish to zero-order.

The calculation centers around the momentum equation and the formulation of the thermal pressure. In FLR theory the zero-order pressure is in general anisotropic and is given by the tensor

$$\mathsf{P}^{(o)} = p_{i\perp}\,\mathsf{I} + (p_{i\parallel} - p_{i\perp})\,\mathbf{BB}/B^2 + p_e\,\mathsf{I} \tag{A3}$$

where $p_{i\perp}$ and $p_{i\parallel}$ are the perpendicular and parallel ion pressures, respectively, and $p_e$ is the isotropic electron pressure. Here we limit the discussion to the case where the upstream is isotropic. Then the anisotropy in (A3) appears only to first order and may be represented by the perturbation anisotropy

$$\delta = (p_{i\perp} - p_{i\parallel})/p_i \tag{A4}$$

The total pressure is given by $\mathsf{P} = \mathsf{P}^{(o)} + \mathsf{P}^{(1)}$, with the FLR terms [*Braginskii,* 1965; *Macmahon,* 1965]

$$\begin{aligned}
{\mathsf{P}_{xx}}^{(1)} &= \frac{\eta}{2}\left(1 + 3\cos^2\theta_{Bn}\right)\left(B_y v_z' - B_z v_y'\right)/B_o \\
{\mathsf{P}_{xy}}^{(1)} &= \frac{\eta}{2}\left(1 - 3\cos^2\theta_{Bn}\right)\cos\theta_{Bn}\, v_z' \\
{\mathsf{P}_{xz}}^{(1)} &= -\frac{\eta}{2}\left(1 - 3\cos^2\theta_{Bn}\right)\cos\theta_{Bn}\, v_y'
\end{aligned} \tag{A5}$$

In the above, $\eta = \frac{1}{2}\left(p_{io}/v_{Ao}\right)\left(c/\omega_p\right)$, and derivatives of $v_x$ as well as variations of the density $\rho$, etc., have been neglected consistent with the order. Also, $c/\omega_p$ and the betas always refer to upstream values.

Using Ohm's law, Faraday's law, and Ampere's law in the deHoffmann-Teller frame (HTF), it is easy to show that to zero as well as to first order the transverse flow is field aligned and the propagation speed is $v_{xo} = v_{Ao}\cos\theta_{Bn}$. Carrying out the expansion to first order, the integrated normal component of the momentum equation becomes

$$\Delta B/B_o = \cos^2\theta_{Bn}\,\Delta\rho/\rho_o - \tfrac{1}{2}\beta_i\,\Delta\mathsf{P}_{xx}/p_{io} \tag{A6}$$

where $\Delta B/B_o = \frac{1}{2}\Delta {B_t}^2/B_o$ and $\Delta\rho/\rho_o = -\Delta v_x/v_{xo}$ from the continuity equation. The first transverse momentum equations gives

$$\frac{\Delta\rho}{\rho_o} = \epsilon + \tfrac{1}{2}\beta_i\left(\sin\theta_{Bn}\cos\theta_{Bn}\sin\alpha\right)^{-1}\frac{\Delta\mathsf{P}_{xy}}{p_{io}} \tag{A7}$$

The second transverse momentum equation provides the same information. The pressure terms can be rewritten as

$$\begin{aligned}
\frac{\Delta\mathsf{P}_{xx}}{p_{io}} &= \left(\gamma_i + \gamma_e\beta_e/\beta_i\right)\Delta\rho/\rho_o + \left(1 - 3\cos^2\theta_{Bn}\right)\delta/3 \\
&\quad - \left(1 + 3\cos^2\theta_{Bn}\right)\sin^2\alpha\;\epsilon/2 \\
\frac{\Delta\mathsf{P}_{xy}}{p_{io}} &= -\cos\theta_{Bn}\sin\theta_{Bn}\sin\alpha\left[\delta + \left(1 - 3\cos^2\theta_{Bn}\right)\frac{\epsilon}{2}\right]
\end{aligned} \tag{A8}$$

Here, the terms multiplying $\epsilon$ represent the FLR corrections (A5), and the terms multiplying $\delta$ are due to the perturbation anisotropy. Also, we have written the isotropic part of the pressure perturbation in terms of adiabatic coefficients $\gamma_i$ and $\gamma_e$, which remain to be specified. The above relations (A6)–(A8), together with an equation for $\delta = \delta(\Delta\rho, \Delta B)$, constitute a set of generally coupled equations for $\Delta B$ and $\Delta\rho$ and specify all perturbations of the plasma within the rotational layer. Note that the amplitude of the deviations from upstream is simply proportional to the rate of rotation $\epsilon = \alpha' c/\omega_p$, and the sign of the perturbation (increase or decrease) reverses with the sense of rotation. As in ideal MHD, both senses of rotation are allowed and so is any-width RD down to the applicability limit of the theory. In the following we discuss a few fluid models of interest.

### Hall-MHD

In this case both the anisotropy and the FLR terms are neglected. This theory should only be valid for quite small values of $\beta_i$, but even there it may not describe the finite beta corrections properly due to the neglect of anisotropy within the layer. The perturbations are in this case

$$\Delta\rho/\rho_o = \epsilon \tag{A9}$$

and

$$\Delta B/B_o = \left(\cos^2\theta_{Bn} - \gamma\beta/2\right)\epsilon \tag{A10}$$

where for simplicity we have written $\gamma_i\beta_i + \gamma_e\beta_e = \gamma\beta$. The change of sign in the magnetic field perturbation occurs at the same critical angle $\cos\theta_c = (\gamma\beta/2)^{1/2}$ that determines the change of helicity and compressibility of the intermediate mode in linear two-fluid theory [*Krauss-Varban et al.*, 1994]. Note that the curve defined by $\theta_c$ is inconsistent with linear kinetic theory for $\beta_i \gtrsim 0.1$–$0.3$ [*Krauss-Varban et al.*, 1994; *Krauss-Varban*, 1994].

The above result of a finite $\Delta B$ may at first appear to contradict the fact that in stationary Hall-MHD $\partial B(x)/\partial x = 0$. This relation derives from the fact that the electron fluid and the transverse ion flow are field aligned if an upstream HTF exists. The paradox can be resolved by taking a closer look at the actual expression for the magnetic field derivative. From Ampere's law we have

$$(c/\omega_p)\,\partial B(x)/\partial x = \sqrt{\rho/\rho_o}(v_z B_y - v_y B_z)/v_A \qquad \text{(A11)}$$

The right-hand side is indeed zero to first order and for $\partial/\partial t = 0$. However, due to the fact that the derivative of $B_o$ is zero and because of the factor $(c/\omega_p)\,\partial/\partial x \simeq (c/\omega_p)\,\ell^{-1} \simeq \epsilon$, the left-hand side is also of second order. In other words, the above equation relates the first-order magnetic field perturbation to second-order terms on the right-hand side. Thus a finite $\Delta B$ is consistent to first order in $\epsilon$, and time variations are a higher order effect. To test this argument that effects due to time variations should be small, we have compared (A9) and (A10) with RD computations using a one-dimensional Hall-MHD code (paper 1). We have found excellent agreement for a wide range of $\beta$ and $\theta_{Bn}$ tested.

### Isotropic FLR-Theory

Although it is inconsistent to neglect anisotropy perturbations when FLR terms are included, we discuss this case here because such a model has been used by *Hau and Sonnerup* [1991]. The resulting equations are

$$\Delta\rho/\rho_o = \left[1 - (1 - 3\cos^2\theta_{Bn})\,\beta_i/4\right]\,\epsilon \qquad \text{(A12)}$$

and

$$\frac{\Delta B}{B_o} = \left\{\cos^2\theta_{Bn} + (1+\cos^2\theta_{Bn})\,\beta_i/4 - \left[1 - (1 - 3\cos^2\theta_{Bn})\,\beta_i/4\right]\gamma\beta/2\right\}\,\epsilon \qquad \text{(A13)}$$

Comparison of $\Delta\rho/\Delta B$ with the values in Table 1 of *Hau and Sonnerup* [1991] gives reasonable agreement as long as the $\Delta$'s are not too large. Some of the perturbations listed in there are quite nonlinear ($\epsilon \gtrsim 2$ based on our $\Delta\rho$). In fact, Hau and Sonnerup's finite width solutions are a direct result of (inconsistently) including the FLR terms to arbitrary order and would not exist unless the FLR terms become large. Similarly, their results that only certain electron sense RDs exist follows from this inconsistency. Instead, as argued above, correct application of first-order FLR theory allows both senses of rotation and arbitrary width down to the limit of applicability, as in ideal MHD and also in agreement with the kinetic hybrid code simulations. As expected, (A12) and (A13) do not conform with our simulation results.

### Alternative Equations of State

The well-known equations of state of the CGL double-adiabatic theory [*Chew et al.*, 1956] may be written $\Delta p_{i\perp}/p_{io} = \Delta\rho/\rho_o + \Delta B/B_o$ and $\Delta p_{i\parallel}/p_{io} = 3\Delta\rho/\rho_o - 2\Delta B/B_o$. Note also that for both temperature components and the total temperature we have $\Delta T_i/T_o = \Delta p_i/p_{io} - \Delta\rho/\rho_o$. Unfortunately, it is immediately evident from our simulations that the above cannot give a reasonable description of kinetic RDs. We find consistently that $T_{i\perp}$ is correlated with $\rho$, regardless of the sign of $\Delta B$ (which is mostly opposite to that of $\Delta\rho$), whereas the above indicates correlation with $\Delta B$. Furthermore, in the simulations $T_{i\parallel} \sim$ const, whereas the above generally results in a finite $\Delta T_{i\parallel}$. We have compared the perturbations resulting after insertion into (A7) and (A8) with our simulations and, as expected, do not find any reasonable agreement. The failure of the double-adiabatic theory is clearly due to the facts that (1) the equations of state are derived assuming zero heat flux, whereas the constancy of $T_{i\parallel}$ indicates the presence of a parallel heat flux; and (2) the above $\Delta T_{i\perp}/T_{io} = \Delta B/B_o$ is equivalent to magnetic moment ($\mu$) conservation, whereas neither in the RD layer nor in the adjacent wave trains of the simulations is $\mu$ actually conserved (compare, e.g., Figures 8 and 9).

Given the findings delineated above, the question arises whether a fluid theory with polytropic coefficients that match the simulation results would fare better. An approximately constant $T_{i\parallel}$ implies a large parallel heat flux, or $\gamma_\parallel \simeq 1$. Also, the variations we measure in the simulations are best described by $\Delta\rho/\rho_o \simeq \frac{3}{2}\Delta T_i/T_o \simeq \Delta T_{i\perp}/T_{io}$. Thus, $\gamma_\perp \simeq 2$. The necessary relations are therefore $\delta = \Delta\rho/\rho_o$ and $\Delta p_i/p_{io} = \gamma_i\,\Delta\rho/\rho_o$ with $\gamma_i = 5/3$. Insertion of these relations into (A6)–(A8) gives the perturbations in this adjusted fluid theory (neglecting FLR terms):

$$\Delta\rho/\rho_o = \epsilon/(1+\beta_i/2) \qquad \text{(A14)}$$

and

$$\frac{\Delta B}{B_o} = \left[\cos^2\theta_{Bn} - (1-\cos^2\theta_{Bn}/2)\,\beta_i - \gamma_e\beta_e/2\right]\epsilon/(1+\beta_i/2) \qquad \text{(A15)}$$

We have not included the standard FLR terms in the above because they are derived assuming validity of the CGL equations of state and zero heat flux, and are therefore not applicable here. Yet, the simulations indicate that modified FLR corrections would improve the fluid theory. Such terms can in principle be calculated from the general third moment equations of Vlasov theory [cf., *Belmont and Rezeau*, 1987] which is, however, beyond the scope of this work. We find (see section 4) that (A15) gives a $|\Delta B|$ that is often a factor two to three too large. The CGL–FLR term in $P_{xx}$ has the ten-

dency to reduce $|\Delta B|$, and indeed $P_{xx}$ in the simulations is qualitatively consistent with such a correction. However, the transverse FLR term (A7) reduces the density perturbation by the factor $[1-(1-3\cos^2\theta_{Bn})\beta_i/4]$, although the simulation $\Delta\rho$ is quite well-described by (A14). In other words, the simulations are qualitatively consistent with the normal component of the standard FLR terms, but not the transverse.

### Asymmetry of Smallest Width

The above theory cannot answer the question of the smallest possible width. However, it is reasonable to assume that an RD ($\ell$) cannot be smaller than the inertial length or the ion gyroradius $\rho_{Li}$, whichever is larger. Realizing that it is the local $\rho_{Li}$ of the layer that is relevant, the above development offers a plausible explanation for the asymmetry of ion sense and electron sense widths. Using $\Delta\rho_{Li}/\rho_{Lio} = \frac{1}{2}\Delta T_{i\perp}/T_{io} - \Delta B/B_o$, (A14), and (A15) results in

$$\frac{\Delta\rho_{Li}}{\rho_{Lio}} = \left[1/2 - \cos^2\theta_{Bn} + (1-\cos^2\theta_{Bn}/2)\,\beta_i + \gamma_e\beta_e/2\right]\epsilon/(1+\beta_i/2) \quad \text{(A16)}$$

Thus, within quasi-perpendicular ion sense RDs ($\epsilon > 0$) the internal $\rho_{Li}$ is elevated, whereas it is reduced for electron sense RDs ($\epsilon < 0$), in agreement with the simulations. Demanding that $\rho_{Li}$ be smaller than $\ell \sim |1/\alpha'|$, (A16) predicts that ion sense RDs should be slightly thicker than the upstream $\rho_{Li}$, whereas electron sense RDs should instead be limited by $c/\omega_p$, except for fairly small $\theta_{Bn}$. While these predictions are in qualitative agreement with the simulation results, one has to keep the limitations of (A15) in mind.

**Acknowledgments.** The authors would like to thank K. B. Quest and C. C. Wu for useful discussions. This work was supported by the Space Physics Theory Program of the National Aeronautics and Space Administration, research grant NAG 5-1492, and NSF grant ATM-9224553. The computations were performed on the Cray Y-MP and C-90 of the the NSF San Diego Supercomputer Center.

The Editor thanks S. Spangler and another referee for their assistance in evaluating this paper.

## References

Belmont, G., and L. Rezeau, Finite Larmor radius effects: The two-fluid approach, *Ann. Geophys., 5A,* 59–70, 1987.

Berchem, J., and C. T. Russell, Magnetic field rotation through the magnetopause: ISEE 1 and 2 observations, *J. Geophys. Res., 87,* 8139–8148, 1982a.

Berchem, J., and C. T. Russell, The thickness of the magnetopause current layer: ISEE 1 and 2 observations, *J. Geophys. Res., 87,* 2108–2113, 1982b.

Braginskii, S. I., Transport processes in a plasma, in *Reviews of Plasma Physics,* vol 1, edited by M. A. Leontovich, pp. 205–311, Consultants Bureau, New York, 1965.

Chew, G. F., M. L. Goldberger, and F. E. Low, The Boltzmann equation and the one-fluid hydromagnetic equations in the absence of particle collisions, *Proc. Roy. Soc. (London), A236,* 112–118, 1956.

Chhajlani, R. K., and S. C. Bhand, Derivation of CGL theory with finite Larmor radius corrections, *J. Plasma Phys., 23,* 205–208, 1980.

Fuselier, S. A., D. M. Klumpar, and E. G. Shelley, Ion reflection and transmission during reconnection at the Earth's subsolar magnetopause, *Geophys. Res. Lett., 18,* 139–142, 1991.

Fuselier, S. A., E. G. Shelley, and D. M. Klumpar, Mass density and pressure changes across the dayside magnetopause, *J. Geophys. Res., 98,* 3935–3942, 1993.

Goodrich, C. C., Numerical simulation of quasi-perpendicular collisionless shocks, in *Collisionless Shocks in the Heliosphere: Reviews of Current Research, Geophys. Monogr. Ser.,* vol. 35, edited by B. T. Tsurutani and R. G. Stone, pp. 153–168, AGU, Washington, D. C., 1985.

Goodrich, C. C., and P. J. Cargill, An investigation of the structure of rotational discontinuities, *Geophys. Res. Lett., 18,* 65–68, 1991.

Gosling, J. T., M. F. Thomsen, S. J. Bame, R. C. Elphic, and C. T. Russell, Plasma flow reversals at the dayside magnetopause and the origin of asymmetric polar cap convection, *J. Geophys. Res., 95,* 8073–8084, 1990.

Gosling, J. T., M. F. Thomsen, S. J. Bame, R. C. Elphic, and C. T. Russell, Observations of reconnection of interplanetary and lobe magnetic field lines at the high-latitude magnetopause, *J. Geophys. Res., 96,* 14,097–14,106, 1991.

Hau, L.-N., and B. U. Ö. Sonnerup, On the structure of resistive MHD intermediate shocks, *J. Geophys. Res., 94,* 6539–6551, 1989.

Hau, L.-N., and B. U. Ö. Sonnerup, Self-consistent gyroviscous fluid model of rotational discontinuities, *J. Geophys. Res., 96,* 15,767–15,778, 1991.

Karimabadi, H., Physics of intermediate shocks: A review, *Adv. Space Res.,* in press, 1995.

Karimabadi, H., and N. Omidi, Hybrid simulations of intermediate shocks: Coplanar and noncoplanar solutions, *Geophys. Res. Lett., 19,* 1723–1726, 1992.

Karimabadi, H., D. Krauss-Varban, and N. Omidi, Kinetic structure of intermediate shocks: Implications for the magnetopause, *J. Geophys. Res.,* this issue.

Krauss-Varban, D., Structure and length scales of rotational discontinuities, *J. Geophys. Res., 98,* 3907–3917, 1993.

Krauss-Varban, D., Bow shock and magnetosheath simulations: Wave transport and kinetic properties, in *Solar Wind Sources of Magnetospheric ULF Waves, Geophys. Monogr. Ser.,* vol. 81, edited by M. J. Engebretson, K. Takahashi, and M. Scholer, pp. 121–134, AGU, Washington, D. C., 1994.

Krauss-Varban, D., N. Omidi, and K. B. Quest, Mode properties of low-frequency waves: Kinetic theory versus Hall-MHD, *J. Geophys. Res., 99,* 5987–6009, 1994.

Lee, L. C., L. Huang, and J. K. Chao, On the stability of rotational discontinuities and intermediate shocks, *J. Geophys. Res., 94,* 8813–8825, 1989.

Lin, Y., and L. C. Lee, Structure of reconnection layers in the magnetosphere, *Space Sci. Rev., 65,* 59–179, 1993.

Macmahon, A., Finite gyro-radius corrections to the hydromagnetic equations for a Vlasov plasma, *Phys. Fluids, 8,* 1840–1845, 1965.

Neugebauer, M., The structure of rotational discontinuities, *Geophys. Res. Lett., 16,* 1261–1264, 1989.

Neugebauer, M., and B. Buti, A search for evidence of the evolution of rotational discontinuities in the solar wind from nonlinear Alfvén waves, *J. Geophys. Res., 95,* 13–20, 1990.

Omidi, N., Rotational discontinuities in anisotropic plasmas, *Geophys. Res. Lett., 19,* 1335–1338, 1991.

Omidi, N., and D. Winske, Kinetic structure of slow shocks:

Effects of the electromagnetic ion/ion cyclotron instability, *J. Geophys. Res., 97,* 14,801–14,821, 1992.

Sonnerup, B. U. Ö., and B. G. Ledley, Ogo 5 magnetopause structure and classical reconnection, *J. Geophys. Res., 84,* 339–405, 1979.

Sonnerup, B. U. Ö., G. Paschman, I. Papamastorakis, N. Sckopke, G. Haerendel, S. J. Bame, J. R. Asbridge, J. T. Gosling, and C. T. Russell, Evidence for magnetic field reconnection at the Earth's magnetopause, *J. Geophys. Res., 86,* 10,049–10,067, 1981.

Swift, D. W., and L. C. Lee, Rotational discontinuities and the structure of the magnetopause, *J. Geophys. Res., 88,* 111–124, 1983.

Vasquez, B. J., and P. J. Cargill, A wave model interpretation of the evolution of rotational discontinuities, *J. Geophys. Res., 98,* 1277–1292, 1993.

Vasyliunas, V. M., Theoretical models of magnetic field merging, 1, *Rev. Geophys. Space Phys., 13,* 303–336, 1975.

Winske, D., and N. Omidi, Hybrid codes: Methods and applications, in *Computer Space Plasma Physics: Simulation Techniques and Software,* edited by H. Matsumoto and Y. Omura, p. 103, Terra Scientific, Tokyo, 1993.

Wu, C. C., Effects of dissipation on rotational discontinuities, *J. Geophys. Res., 93,* 3969–3982, 1988.

Wu, C. C., Formation, structure, and stability of MHD intermediate shocks, *J. Geophys. Res., 95,* 8149–8175, 1990.

Wu, C. C., and T. Hada, Formation of intermediate shocks in both two-fluid and hybrid models, *J. Geophys. Res., 96,* 3769–3778, 1991a.

Wu, C. C., and T. Hada, On rotational discontinuities in both two-fluid and hybrid models, *J. Geophys. Res., 96,* 3755–3767, 1991b.

---

H. Karimabadi, D. Krauss-Varban, and N. Omidi, Department of Electrical and Computer Engineering, University of California at San Diego, Mail Code 0407, La Jolla, CA 92093-0407. (email: varban@ece.ucsd.edu)

(Received August 10, 1994; revised November 1, 1994; accepted November 17, 1994.)